Central Neural Regulation of Parathyroid Hormone

L. Zhang[1, 2 #], N. Liu[1, 2, 3 #], J. Shao[1], D. Gao[1], Y. Liu[1], Di Chen[4], L. Wang[1], W. W. Lu[2,*], F. Yang[1,*]

[1]The Brain Cognition and Brain Disease Institute (BCBDI), Shenzhen Institutes of Advanced Technology, Chinese Academy of Sciences (CAS); CAS Key Laboratory of Brain Connectome and Manipulation; Guangdong Provincial Key Laboratory of Brain Connectome and Behavior; Shenzhen-Hong Kong Institute of Brain Science-Shenzhen Fundamental Research Institutions, Shenzhen 518055, China

[2]Department of Orthopaedics and Traumatology, The University of Hong Kong, Hong Kong

[3]Department of Biomedical Engineering, Southern University of Science and Technology, Shenzhen, Guangdong, China

[4]Research Center for Human Tissues and Organs Degeneration, Shenzhen Institutes of Advanced Technology, Chinese Academy of Sciences

[#]These authors contributed equally to this work

*Corresponding author: William W Lu, PhD, University of Hong Kong, wwlu@hku.hk, Fan Yang, PhD. Shenzhen Institutes of Advanced Technology, fan.yang@siat.ac.cn;

Abstract

Parathyroid hormone (PTH) is one of the most important hormones responsible for bone turnover and calcium homeostasis, however, the mechanism underlying central neural regulation of PTH in mammals remains largely unknown. In this study, we identified the subfornical organ (SFO) and the paraventricular nucleus (PVN) as two important brain nuclei responded to serum PTH and calcium changes. Using chemogenetics, we

found that serum PTH was suppressed by stimulation of SFO^{GABA} neurons followed by a decrease in trabecular bone mass. Conversely, stimulation of SFO^{VGlut} neurons promoted serum PTH and bone mass. The paraventricular nucleus (PVN) is downstream of the SFO, and chemogenetic activation of PVN^{CaMKII} and PVN^{VGlut} neurons induced an increase in serum PTH. These findings reveal important central neural nodes and will advance our understanding of the central neural regulation of PTH at the molecular, cellular and circuit level.

Keywords: Parathyroid; subfornical organ; bone

Introduction

Parathyroid hormone (PTH) is one of the most important hormones that modulate bone remodeling and calcium homeostasis, which is conserved from zebrafish to humans(Wein and Kronenberg, 2018, Suarez-Bregua et al., 2017a). In fish that do not have isolated parathyroid glands, PTH peptides are mainly expressed in the lateral line, the neural tube and in the central nervous system(Canario et al., 2006, Liu et al., 2010, Suarez-Bregua et al., 2016). In humans and other mammals, PTH is mainly secreted from the parathyroid glands to maintain basal serum calcium levels under different nutrient conditions. The secretion of PTH is finely regulated by the humoral, hormonal stimulations, and the level of PTH is precisely maintained based on the serum calcium concentration.

In the mammalian central nervous system (CNS), parathyroid hormone 2 receptors (PTH2R) and TIP39 proteins form a unique neuropeptide–receptor system, in which there is a wide distribution of axon terminals from neurons that support functions such

as nociceptive signaling and neuroendocrine regulation(Dobolyi et al., 2010). In the rat brain, PTH2-receptor expression is observed in the cerebral cortex, stratum and hypothalamus, including the arcuate nuclei and median eminence(Wang et al., 2000). Recent work showed that ancient parathyroid hormone 4 (PTH4) is a central neural regulator of bone development and mineral homeostasis(Suarez-Bregua et al., 2016), and ablation of PTH4 neurons results in abnormal bone mineralization and osteoblast differentiation in zebrafish(Suarez-Bregua et al., 2017b). These findings support that PTH or PTH receptors might have played a continuous prominent role in the brain-to-bone signaling pathway and in the maintenance of bone homeostasis during vertebrate evolution. However, whether the adult mammalian central nervous system has retained the capacity to detect PTH levels and direct the neural regulation of PTH homeostasis is largely unknown.

In addition to the CNS, abundant levels of neural terminal expression have been observed in parathyroid glands(Shoumura et al., 1983, Romeo et al., 1986, Mortimer et al., 1990, Egawa and Kameda, 1995, Luts et al., 1996, Chen et al., 2005). Administration of epinephrine or isoproterenol infusion acutely induces PTH release, which is ablated by the β-adrenergic receptor 2 antagonist propranolol(Fischer et al., 1973), and direct stimulation of parathyroid nerves upstream of the parathyroid induces serum PTH elevation(Hotta et al., 2017a). Clinical studies have also shown that neuropsychiatric symptoms including anxiety, depression and cognitive impairments are prevalent in patients with hyperparathyroidism, which, along with bone abnormalities, are significantly improved after parathyroidectomy(Chou et al., 2008, Liu et al., 2020). Based on this evidence, we hypothesized that distinct brain nuclei and neuronal subtypes may sense PTH levels and direct peripheral nerves to regulate PTH

secretion in a top-down manner. However, it is not clear what these important nodes in the central nervous system that control PTH secretion in mammals are, or the underlying mechanisms.

In this study, we firstly identify the subfornical organ (SFO), a member of the circumventricular organs (CVO), as an important brain nucleus modulating the homeostasis of PTH. Chemogenetic activation of SFO^{VGlut} and SFO^{GABA} neurons exerted responses in opposing directions in serum PTH and tibiae trabecular bone mass. Neurons in the SFO express PTH receptors 1 and 2, the majority of which are expressed in SFO^{GABA} and SFO^{VGlut} neurons, respectively. Activation of paraventricular nucleus $(PVN)^{VGlut}$ neurons, which are downstream of the SFO, led to elevated PTH and trabecular bone mass. In addition, sympathetic and sensory nerves were identified within the parathyroid glands, and ablation of these affected serum PTH levels and PTH response to calcium. Our study not only demonstrates that the central nervous system is indispensable for the regulation of peripheral PTH secretion and maintenance of bone-metabolism homeostasis, but also for the first time revealed the underlying mechanism of central neural regulation of the PTH at molecular, cellular and circuit level.

Results

Parathyroid glands are connected to the central nervous system

Previous studies have demonstrated that parathyroid glands (PTG) receive sympathetic parasympathetic and sensory neural innervation, however, the central source of this innervation was not clear. To determine the brain nucleus that innervates the parathyroid gland (PTG), we injected the neural retrograde tracer pseudorabies virus (PRV-GFP)

directly into the PTG (Fig. 1A-C). The brain nuclei with the highest PRV expression markers included: the median preoptic nucleus (MnPO), medial preoptic nucleus, lateral part (MPOL), subfornical organ (SFO), suprachiasmatic nucleus (SCh) the nucleus of the vertical limb of the diagonal band (VDB) , and area postrema (AP) (Fig. 1B, Fig. S1). The MnPO, SFO and AP belongs to a group called the circumventricular organs (CVO), which are characterized by their extensive and highly permeable microvasculature and have no blood-brain-barrier(McKinley et al., 2003).

To investigate the brain nuclei responsive to peripheral PTH, we injected calcium chloride, human PTH (1-34) or saline intravenously into C57 mice (Fig 1D). Neuronal activation was assessed following cFos immunostaining, and cFos positive cells were quantified in different brain nuclei. We found that neurons in a variety of brain nuclei, including the SFO, paraventricular thalamic nucleus (PVN), anterior paraventricular thalamic nucleus (PVA) and SCh were activated by serum PTH (Fig. S2), and the number of cFos positive cells in the SFO and PVN significantly increased after PTH injection (Fig. 1F).

We then performed a PTH-Biotin binding assay to determine whether peripheral PTH can enter the central nervous system and bind directly to specific brain nuclei. Positive PTH-Biotin binding sites were detected using immunofluorescence staining of Biotin, and included the SFO, periventricular hypothalamic nucleus (pv), SCh, periventricular hypothalamic nucleus (Pe), AP and the nucleus tractus solitarius (NTS) (Fig. 1E, Fig. S3). The majority of identified nuclei were located surrounding the brain ventricles. Joborn and colleagues reported high-level expression of PTH in human cerebrospinal fluid, especially in hyperparathyroidism patients(Joborn et al., 1991) and our results

support this by showing that peripheral PTH can indeed enter the central nervous system and bind to specific brain nuclei. This finding provides evidence that the CNS senses PTH signals from the circulation which serves as the physiological basis for negative or positive feedback of central neural regulation of PTH.

Using the three above-mentioned methodological approaches, we identified the SFO as one prominent brain nucleus that is both physically and functionally connected to the parathyroid gland. The SFO is an important area in the forebrain, a member of the sensory circumventricular organs (sCVO)(McKinley et al., 2003), which play an important role in the regulation of water and sodium intake(Zimmerman et al., 2017). To further confirm the direct effects of PTH on SFO neurons, we used patch clamp recordings to observe the direct neuronal response to PTH. Application of PTH (10^{-6} M) led to significantly increased SFO neuron resting potentials and firing rates (Fig. 1G). In summary, these results demonstrate that the parathyroid glands receive synaptic connections from a variety of brain nuclei, and that SFO neurons directly respond to peripherally administered PTH.

Activation of SFO^{GABA} and SFO^{VGlut} neurons have different effects on the regulation of PTH and bone remodeling

Neurons in the SFO detect serum nutrients and osmotic pressure directly through leaky blood vessels and regulate drinking and feeding behavior through downstream nuclei(Oka et al., 2015, Vivas et al., 1990, Anderson et al., 2000, Zimmerman et al., 2016, Matsuda et al., 2017). To investigate whether neural activity of the SFO modulates serum PTH levels, we activated SFO neurons directly using chemogenetics and analyzed serum PTH changes (Fig. 2A). Because calmodulin-dependent protein

kinase II (CaMKII) was previously identified as a marker of excitatory neurons in the SFO(Oka et al., 2015, Nation et al., 2016), we firstly activated SFO^{CaMKII} neurons by injecting AAV9-CaMKII-hM3Dq-mCherry/AAV9-CaMKII-mCherry viruses into the SFO and then used Clozapine-N-oxide (CNO) to activate SFO^{CaMKII} neurons (Fig. 2A). There was significantly lower serum PTH (23.6% lower) in the hM3Dq group following activation of SFO^{CaMKII} than in the control group, but no difference in serum calcium levels (Fig. 2A). After chronic stimulation for 4 weeks, bone mineral density (BMD) of the tibiae trabecular was 19.6 % lower than the control group, accompanied by lower trabecular bone volume fraction (BV/TV) and trabecular number (Tb.N; Fig. S4A). However, the BMD of cortical bone was similar between groups (Fig. 2A).

Previous studies have indicated that the SFO contains intermingled populations of glutamatergic (SFO^{GLUT}) and GABAergic (SFO^{GABA}) neurons, one which triggers and one which curbs thirst(Oka et al., 2015). To explore whether glutamatergic and GABAergic neurons are involved in regulating PTH, we investigated colocalization of CaMKII with gamma-aminobutyric acid (GABA) and vesicular glutamate (VGlut). We found that 32.2% of AAV9-CaMKII-mCherry-labeled neurons expressed GABA in the SFO, whereas 59.7% of CaMKII-labeled neurons colocalize with VGlut (Fig. 2B). We then assessed colocalization of cFos expression and *vglut2/gad1&2* expression in SFO induced by peripheral PTH (Fig. 2C). Of the SFO neurons activated following peripheral PTH application, we found an intermingled mixture with 43% glutaminergic and 45% GABAergic neurons (data not shown), suggesting that both type of neurons can be activated by PTH.

To further investigate the regulatory function of GABAergic and glutamatergic neurons

in the SFO, we performed chemical genetic stimulation using the AAV9-GAD-cre virus and the AAV9-DIO-hM3Dq system (Fig. 2D), and we found that specific stimulation of SFO^{GABA} neurons induced a significant decrease of PTH (32.1%) and tibiae trabecular BMD (20.7%), whereas serum calcium levels and cortical BMD were not significantly different from controls (Fig. 2D, Fig. S4B). Similarly, we used VGlut2-Cre mice and the AAV9-DIO-hM3Dq system to stimulate SFO^{Glut} neurons, and chemogenetic stimulation resulted in a 55.9% increase of serum PTH and 38.7% increase in tibia trabecular BMD accompanied by a significant increase in BV/TV and trabecular numbers (Fig. 2E, Fig. S4C). These results demonstrate that SFO^{GABA} and SFO^{Glut} neurons both regulate serum PTH levels and bone metabolism, indicating that the CNS bilaterally regulates PTH through isolated pathways. However, the effects of these two distinct neuronal populations on the regulation of PTH secretion and bone remodeling appear counter each other.

PTH receptors expressed in SFO neurons regulate negative feedback of PTH secretion

Since peripheral PTH can directly bind and activate SFO neurons (Fig. 1E-F), we next assessed PTH-receptor expression in the SFO and their function in the regulation of serum PTH. Immunofluorescence analysis revealed that PTH1R expression was colocalized with PTH-induced cFos expression in the SFO, as was PTH2R expression (Fig. 3A, B).

Neurons expressing PTH2R are widely distributed in the central nervous system, and their functions in the locus coeruleus (LC), amygdala, and the periaqueductal gray (PAG) are correlated with pain and nociceptive behaviors(Dobolyi et al., 2012,

Dimitrov et al., 2013, Tsuda et al., 2015). Expression of PTH1R in the SFO was demonstrated by *in situ* hybridization in the Allen Brain Atlas (Pth1r-RP_110421_01_D07-coronal). However, PTH1R function in the brain has not been studied in detail. To investigate the function of the PTH1R and PTH2R in maintaining PTH homeostasis, we down-regulated PTH1R and PTH2R expression in the SFO using LV-PTH2R-Cas9 and LV-PTH1R-Cas9, respectively (Fig. 3C). Basal levels of PTH and calcium were not affected by knockdown of PTH2R and PTH1R in the SFO (Fig. 3E). However, response to exogeneous calcium/human PTH (1-34) stimulation was affected after the down regulation of PTH1R receptors (Fig. 3D). During PTH tolerance tests, serum calcium significantly increased in the control and PTH2R knockdown groups following exogenous hPTH (1-34) stimulation. However, serum calcium levels were not affected in the PTH1R knockdown group and endogenous PTH did not change compared to the control group during this process (Fig. 3D, upper panel). During a calcium tolerance test, serum PTH decreased within 30 mins after calcium administration in control group. However, serum PTH did were not affected in PTH1R knockdown group. The serum calcium in the PTH1R knockdown group is also remarkedly higher than control. A calcium tolerance test during PTH2R knockdown led to a reduction of PTH, yet there was a sharp elevation of serum calcium in the fifth minute, compared to controls, which returned to baseline levels, suggesting that PTH2R may affect serum calcium through a mechanism other than the direct regulation of serum PTH (Fig. 3D, lower panel).

In order to tease apart PTH1R/PTH2R expression in glutamatergic and GABAergic neurons in the SFO, we used colocalization staining and found that PTH1R and PTH2R were both expressed in SFO^{Glut} and SFO^{GABA} neurons (Fig. 3F, Fig. 3H). Quantification

revealed that the majority of cells that expressed PTH1R were GABAergic (81.0%) compared to glutamatergic neurons (53%) (Fig. 3G). Conversely, the majority of PTH2R cells were glutamatergic (73.7%) compared to GABAergic neurons (54.4%) (Fig. 3I).

We also performed behavioral tests and found that knockdown of PTH1R expression induced a slight increase of open-arm time in an elevated plus maze (EPM). In an open-field test (OFT), time spent in the central area was not affected and neither was immobility time in a tail suspension test (TST) during knock down of PTH1R or PTH2R (Fig. S6A). In fluid consumption tests, knock down of PTH1R and PTH1R induced a preference of more water compared to NaCl. However, total fluid consumption was not affected (Fig. S6B).

To further gain more insight into SFO^{PTH2R} neuron function, we constructed a PTH2R-$CreER^{T2}$ transgenic mouse strain (Fig. S7A). Colocalization staining with NeuN demonstrated that the majority of $PTH2R^{+}$ cells in the SFO are neurons (Fig. S7B). Chemogenetic activation of PTH2R neurons in the SFO resulted in a 20.9% increase in serum PTH, which is consistent with the above activation of SFO^{VGlut} neurons. However, trabecular and cortical BMD was not affected (Fig. S7C, D). Activation of SFO^{PTH2R} neurons also resulted in less time spent in the central area in an OFT, whilst open-arm time in an EPM and immobility time in a TST was not affected. Activation of SFO^{PTH2R} also led to a higher intake of water compared to the control group (Fig. S7E).

In summary, we have demonstrated that PTH receptors in the SFO, PTH1Rs in

particular, play important roles in the regulation of PTH and calcium homeostasis in response to exogenous hPTH(1-34) and $CaCl_2$ stimulations. Our data support that the SFO is important for both sensing PTH/calcium levels and for the regulation of PTH secretion.

PVN regulation of PTH

Next, we investigated the downstream effectors of SFO neurons. We know that SFO^{CaMKII} neurons project to a variety of brain nuclei including the MnPO, paraventricular nucleus (PVN), Vascular organ of lamina terminalis (OVLT) and bed nucleus of the stria terminalis (BNST)(Zimmerman et al., 2017) (Fig. S5). Of these brain nuclei, the PVN is reported as crucial in the regulation of both neuroendocrine homeostasis and sympathetic activity. Since serum PTH is regulated through the sympathetic nervous system(Fischer et al., 1973, Hotta et al., 2017b), we investigated whether PVN neurons are involved in the regulation of PTH and bone metabolism.

Unlike the SFO, which consists of both GABAergic and glutamatergic neurons, we found that the majority of PVN neurons responding to peripheral PTH stimulation (cFos-positive) were colocalized with *vglut2* and not *gad1&2* (Fig. 4A). Immunofluorescence showed that CaMKII and VGlut2 are both abundantly expressed in the PVN. Quantification revealed that VGlut2/CaMKII double-positive cells accounted for 62.6% of VGlut2-positive neurons, and 67.7% of CaMKII-positive neurons (Fig. 4B).

Next, we investigated the regulatory functions of PVN^{CaMKII} and PVN^{VGlut} neurons. Chemogenetic activation of PVN^{CaMKII} neurons in the hM3Dq group resulted in a 62.2%

higher serum PTH level than the mCherry group. However, there was no difference in the BMD of trabecular or cortical bone between groups (Fig. 4C, Fig. 4E, Fig. S8A). Similarly, we activated PVN^{VGlut} neurons after injecting the AAV9-DIO-hM3Dq-mCherry into the PVN of VGlut2-Cre mice (Fig. 4D) and found that chronic activation of PVN^{VGlut} neurons led to significantly higher serum PTH than the control group (53.7%), and a higher trabecular BMD in mice tibiae (27.4%) (Fig. 4D, Fig. 4F). Both trabecular thickness and trabecular number were also significantly higher in the experimental group (Fig. S8B). These data suggest that the activation of glutamatergic neurons in PVN efficiently up-regulate PTH levels and bone remodeling.

GABAergic neurons in the SFO send neuronal projections to the PVN and innervate glutamatergic neurons in the SFO

Direct SFO^{CaMKII} projection to the PVN has been observed by Zimmerman et al. (2016). However, it is not known whether the PVN receives an SFO^{GABA} projection. We studied SFO^{GABA} neuronal projections using a combined injection of AAV9-DIO-mCherry and AAV9-GAD67-Cre viruses into the SFO of C57 mice. In addition to the previously described SFO^{GABA}→MnPO and SFO^{GABA}→OVLT neuronal projection(Matsuda et al., 2017, Oka et al., 2015), we found that the PVN also receives dense innervation from SFO^{GABA} neurons (Fig. 5A). To confirm that the PVN^{VGlut2} neurons specifically receive synaptic connections from SFO^{GABA} neurons, we performed retrograde tracing by injecting AAV9-TVA-RVG and RV-ΔG-mCherry into the PVN of VGlut2-Cre mice (Fig. 5B). Efficient transfection of AAV helper and RV in PVN glutamatergic neurons was indicated by mCherry signals in the PVN. In the SFO, RV positive mCherry signals, which were colocalized with GABA and CaMKII, indicated retrograde monosynaptic connection with PVN^{VGlut2} neurons (Fig. 5B).

To explore regulatory function in SFO^{GABA} → PVN neurons, we injected AAV9-GAD67-Cre virus into the SFO and AAV2retro-DIO-hM3Dq-mCherry virus into the PVN of C57 mice. Specific activation of the neural projections from SFO^{GABA} -PVN circuit did not affect serum PTH and calcium levels but induced a 12.3% lower tibiae trabecular BMD in the hM3Dq group (Fig. 5C, D). Time spent in the open arm of the EPM was slightly higher in the hM3Dq group, whilst there was no group difference either in time in the center during OFT or immobility time in TST during activation of the circuit. In addition, fluid intake was similar between groups (Fig.S9B). These results reveal a novel SFO^{GABA}-PVN circuit which mainly regulates trabecular bone metabolism.

Ablation of sympathetic nerves affect serum PTH level

Innervation of parathyroid glands has been reported in previously studies. In our study, we observed both the sympathetic nerves (TH^+) and sensory nerves which were labeled with calcitonin gene related protein ($CGRP^+$) in the parathyroid gland (Fig. 6A). Double staining revealed sympathetic nerves in mice parathyroid glands, which form a net-like structure that surrounds the blood vessels ($CD31^+$); the sympathetic nerves form clusters with blood vessels rather than an even distribution in the parathyroid glands (Fig. 6A). On the other hand, most CGRP nerves were observed between parathyroid-gland substructures as single neural fibers (Fig. 6A).

Physical connectivity between the parathyroid glands and the nervous system was also investigated using neuronal-specific retrograde tracing from the parathyroid glands. We injected CTB-Alexa Fluor 488 into one side of the rat parathyroid glands and then after

sacrifice, both side of the sympathetic superior cervical ganglia (SCG) and inferior vagal ganglia (Vagus) were isolated to study innervation. CTB signals were observed in both sides of the SCG and Vagus. These results are consistent with the findings of both sympathetic nerves and CGRP nerves in parathyroid glands (Fig. 6B, Fig. 6C).

Next, we performed RV tracing using PTH-Cre mice to assess whether there is direct synaptic connectivity between parathyroid chief cells and the peripheral nervous system. The signals of both RV and helpers were observed in parathyroid glands in PTH-Cre mice, indicating that the AAV helper and RV had infected parathyroid chief cells (Fig. 6d). One week after virus infusions, positive RV signals were observed in the SCG and Vagus following counterstaining of tyrosine hydroxylase (TH) in the SCG, and choline acetyltransferase (ChAT) and calcitonin gene-related protein (CGRP) in the Vagus (Fig 6E). These results indicate that the SCG and Vagus may be directly connected to the parathyroid chief cells by direct, monosynaptic connections.

The function of peripheral sympathetic nerves in the regulation of PTH was investigated further through ablation of peripheral sympathetic neural terminals by 6-OH-Dopa administration (*i.p.)* in mice and into the parathyroid glands in rats (Fig. 6F). Universal ablation of sympathetic neural terminals in mice induced a decrease of basic serum PTH and calcium (Fig. 6F, upper panel), whereas in rats with local ablation of sympathetic neural terminals, there was no change (Fig. 6F, lower panel). Both universal ablation of sympathetic innervation in mice and specific ablation of sympathetic nerve terminals in rat parathyroid led to significantly attenuated serum PTH changes in response to high calcium stimulation (Fig. 6F).

In summary, these data demonstrate that the sympathetic and sensory nervous system are both tightly integrated with the parathyroid glands, and that the ablation of peripheral sympathetic nerve significantly impacts PTH response to high calcium challenge.

Discussion

Modulation of serum calcium levels and bone remodeling relies upon serum PTH, the most important hormone in this regard, levels of which are maintained through humoral, hormonal and neural regulation(Munger and Sheppard, 2011). However, until now the effects of central neural regulation of serum PTH and underlying mechanisms were largely unknown. Using neural circuit tracing and chemogenetic techniques in addition to analysis of PTH and bone metabolism, we for the first time, systemically studied the structural and functional connection between the parathyroid and specific types of neurons in the central nervous system. This resulted in the identification of the components of a specific central neural circuit that modulates PTH and in the revelation of the underlying mechanism of central neural regulation of PTH levels and bone metabolism (Fig. 6G).

Central nervous system (CNS), PTH and bone metabolism

The close relationship of PTH to the CNS has been observed for decades. The earliest studies suggesting PTH function within the CNS stem from a series of findings beginning with the identification of PTH-like immunoreactive protein in the brains of different species, particularly in bony fish. In mammals, the embryonic origin of parathyroid gland is derived from the 3rd and 4th brachial pouch, which closely neighbors the neural crest (NC) mesenchyme(Policeni et al., 2012, Bain et al., 2016).

An evolutionary model has also been proposed, in which, during the evolutionary period where aquatic vertebrates transitioned to a terrestrial environment, the parathyroid gland gradually migrated from the CNS to the periphery to enhance calcium regulatory capacity during times of unstable calcium dietary supplementation(Suarez-Bregua et al., 2017a). However, the question of whether the CNS still reserves calcium and PTH regulation functionality in adult mammals has never been asked. In this study, we provide the first demonstration that chemogenetic activation of SFO^{GABA}, SFO^{VGlut}, PVN^{CaMKII} and PVN^{VGlut} neurons are able to directly modulate serum PTH levels and the bone metabolism in the absence of any other experimental manipulation. Conversely, knocking down expression of PTH1R and PTH2R in the SFO, or ablation of the sympathetic nerves in the PTG, led to a significant blockade of serum PTH and calcium responses to exogenous calcium and PTH stimulation, but did not affect baseline PTH level. This evidence demonstrates the necessity of the central and peripheral nervous systems in both regulating PTH basal secretion and maintaining PTH homeostasis through feedback loops.

Parathyroid hormone is an important hormone in the bone remodeling process, where it initiates bone resorption followed by bone formation(Wein and Kronenberg, 2018). Ablation of PTH4 neurons result in abnormal bone mineralization and significantly affects osteoblast differentiation(Suarez-Bregua et al., 2017b), suggesting that PTH might be an important regulator of the central neural control of bone remodeling. In our study, we found that changes in bone mass were typically in the same direction as PTH changes; that is, decreased PTH was followed by decreased tibiae trabecular BMD and increased PTH was followed by increased tibiae trabecular BMD. Previous studies have indicated that intermittent administration (daily) of PTH induces an anabolic effect in

bone, which is contrary to the effects of continuous administration(Wein and Kronenberg, 2018). In our study, chemogenetic activation of brain neurons was performed with transduction of hM3Dq in the brain and administration of CNO (*i.p.*) every 48 hours. Based on a pharmacokinetic study of CNO(Jendryka et al., 2019), serum PTH changes induced by chemogenetic stimulation of mice reached peak levels every 48 hours, which may explain the anabolic effects of PTH on bone.

SFO neurons are important in both the detection and regulation of PTH level

As a member of the CVO, the SFO directly detects circulating molecular signals in serum. We found PTH1R and PTH2R expression in SFO neurons, reaffirming this finding reported in the Allen Brain Atlas database. The binding efficiency of PTH1R to PTH is different from that of PTH2R. The EC50 of PTH1R to PTH (1-34) is around 1-2 nM, whereas the EC50 of PTH2R to PTH (1-34) is around 70 nM(Usdin et al., 1999). Therefore, serum PTH in healthy individuals (65-150 pg/mL) would likely predominantly activate only PTH1R in the SFO. In our study, we found that PTH1R expression was predominant in SFO^{GABA} neurons and activation of SFO^{GABA} neurons induced a decrease in serum PTH. It is thus expected that, under physiological conditions, the CNS can modulate serum PTH in a negative feedback pathway mainly through SFO^{GABA} neurons.

On the other hand, under severe pathological conditions such as hyperparathyroidism (HPT), serum PTH levels are around 10-100 times higher than physiological levels and SFO^{VGlut} neurons, which mainly expressed PTH2R, would be activated to induce a consistent increase of serum PTH. Our study indeed found that activation of the SFO^{Vglut2} neurons did induce a significant elevation of PTH levels and lowered bone

density, which is a reverse of the regulatory effects of SFO^{GABA} neurons. Our findings may thus explain why serum PTH becomes uncontrollable in patients of late-stage HPT and leaves them with no other treatment except parathyroidectomy surgery.

In addition, it is consistently reported that HPT patients develop psychiatric symptoms including anxiety, depression and cognitive disorder(Joborn et al., 1986). Moreover, if these symptoms develop in primary or secondary HPT diseases, they improve following parathyroidectomy surgery(Kollars et al., 2005, Roman et al., 2011, Driessen et al., 1995, Chou et al., 2008). The function of PTH2R and the agonist TIP39 mediate nociception, including neuropathic and inflammatory pain(Dimitrov et al., 2013); genetic knockdown of PTH2R in the medial amygdala and disruption of PTH2R projections to the bed nucleus of the stria terminalis (BNST) influence fear- and anxiety-like behavior (Fegley et al., 2008, Tsuda et al., 2015). However, there are no gain of function studies for PTH2R reported in the literature. In our study, we firstly found that knockdown of *pth2r* in the SFO did not induce behavioral changes. However, chemogenetic activation of SFO^{PTH2R} neurons in PTH2R-creERT2 mice led to less time in the center during OFT tests, which is used as an index of anxiety, even although immobility time during TST was not affected. These data indicate that PTH2R neurons in the SFO regulate anxiety-like behaviors in mice, in addition to regulating PTH level and the bone remodeling process.

The PVN, sympathetic nerves and the PTH

Of the nuclei downstream of the SFO, we chose the PVN as the target to study its function in the regulation of PTH. In addition to the fact that PVN receives polysynaptic connections from the PTG and is responsive to peripherally administrated PTH and

calcium, the PVN receives a direct monosynaptic neural projection from SFO GABAergic neurons as revealed by our RV tracing study. The PVN is well known as crucial member of the neural-humoral hypothalamic-pituitary-thyroid (HPT) axis and the hypothalamic-pituitary-adrenal (HPA) axis(Swanson and Sawchenko, 1983). In addition, PVN^{VGlut} neurons also directly project to the nucleus tractus solitarius (NTS), which affects sympathetic nerves through a neural sympathetic connection(Kawabe et al., 2008); activation of PVN^{VGlut} neurons increase the activity of the sympathetic nervous system(Shi et al., 2020).

By directly activating PVN neurons, we firstly found that activation of PVN neurons results in elevated serum PTH levels, and found different regulatory effects following activation of PVN^{CaMKII} or PVN^{VGlut} neurons, despite overlap of these neurons. Activation of both PVN^{CaMKII} and PVN^{VGlut} induced an increase in serum PTH, however, trabecular BMD was not affected following PVN^{CaMKII} activation yet increased following PVN^{VGlut} activation. These findings suggest that PVN^{VGlut} neurons are more likely to regulate both PTH levels and bone metabolism compared to PVN^{CaMKII} neurons, since PVN^{VGlut} neurons directly receive a monosynaptic projection from SFO^{GABA} neurons. Previous research has indicated that noradrenergic neurons in the PVN suppress stress-induced bone loss(Baldock et al., 2014), whereas our study shows that PVN^{VGlut} neurons exerted more of an effect on bone metabolism through the regulation of PTH. The inhibitory effects on trabecular bone BMD following specific activation of the GABAergic neural projection from the SFO to the PVN further confirmed that PVN can relay upstream signals from the SFO to regulate bone metabolism (Fig. 5).

Previous work has indicated that serum PTH increased tenfold during electric stimulation of the cerebral sympathetic trunk (CST)(Hotta et al., 2017a). Consistent with this, we found that ablation of peripheral sympathetic nerves in mice induced a significant decrease of serum PTH. This finding is also consistent with an earlier study in which direct infusion of epinephrine induced 127 to 255% increase of PTH in cows(Fischer et al., 1973). From our immunofluorescence study, we found that TH nerve terminals were tightly surrounded by the capillaries within the PTG, indicating that serum PTH may be regulated sympathetically via capillary vasodilation and contraction. The neural tracing experiments and ablation study further confirmed that sympathetic innervation is necessary for relaying the central signals to regulate PTH homeostasis.

In summary, our contributions are in three parts. Firstly, we identified the SFO and PVN as important nodes that regulate serum PTH levels and bone metabolism. Secondly, for the first time, we revealed a population of GABAergic neurons in the SFO, which not only detect PTH levels via PTH receptors, but also directly regulates PTH levels. Thirdly, we found that the PVN and peripheral sympathetic system were downstream of the SFO in this circuit and play important roles in the regulation of PTH homeostasis and bone metabolism. Therefore, not only did we identify the underlying mechanism of central neural regulation of serum PTH, but also provide evidence of the intricate process by which the CNS detects peripheral PTH and the responses to changes in serum PTH under physiological or pathological conditions.

Acknowledgements

This project was partly supported by the National Natural Science Foundation of China

(81471164); Key Research Program of Frontier Sciences of Chinese Academy of Sciences (QYZDB-SSW-SMC056); Shenzhen Governmental Basic Research Grant (JCYJ20170413164535041, JCYJ20180507182301299)

Author contributions:

Fan Yang, William W Lu, Liping Wang, Di Chen supervised the study. Lu Zhang, Nian Liu designed the experiments and conducted chemogenetic experiments, animal behavior studies, serum biochemical analysis and analyzed data. Jie Shao performed electrophysiological recordings in brain slices Dashuang Gao performed PRV retrograde tracing experiments. Yunhui Liu performed sympathetic nerve ablation test.

Declaration of interests: The authors have declared that no conflict of interest exists.

Figure legends

Figure 1. Parathyroid glands are connected to the SFO and PVN.

A, Schematic showing pseudorabies virus (PRV) infection of SD rat parathyroid gland (PTG) and poly trans-synaptic connection to the central nervous system. **B**, PRV expression density in different rat brain areas after PRV neural tracing (No./mm^2, n=3). 2n, optic nerve; Arc, arcuate nucleus; IRT, intermediate reticular nucleus; IO, inferior olive; LH, lateral hypothalamic area; LPO, lateral preoptic area; MnPO, median preoptic nucleus; MnR, median raphe nucleus; NTS, nucleus tractus solitarius; PAG, periaqueductal gray; PnV, pontine reticular nucleus ventral part; PVN, paraventricular thalamic nucleus; SFO, subfornical organ; SCh, suprachiasmatic nucleus; VDB, nucleus of the vertical limb of the diagonal band. **C**, PRV positive signals in the PTG (***left,*** scale bar, 50 μm), SFO (***middle,*** scale bar, 100 μm) and PVN (***right,*** scale bar, 100

μm). **D**, Schematic showing peripheral administration of PTH (1-34), $CaCl_2$ and PTH-biotin. **E**, Peripherally administrated PTH-Biotin (green florescence) binds to the SFO; PTH without biotin was a negative control. Scale bar, 100 μm. **F**, cFos expression in the SFO (***upper left,*** scale bar, 100 μm) and PVN (***lower left,*** scale bar, 100 μm) after peripheral $CaCl_2$ or PTH administration. Quantification of cFos positive cells in the SFO and PVN (***right***, n=3). **G**, Electrophysiological recording of SFO cells with whole-cell patch (n=8). RPM, resting membrane potential, P analyzed by paired two-tailed t-test. All error bars and shaded areas show mean ± s.e.m.

Figure 2. SFO neurons regulate serum PTH level.

A, Chemogenetic stimulation of CaMKII neurons in the SFO of C57 mice (n=9). ***Left***, injection of AAV-CaMKII-hM3Dq/mCherry into the SFO of C57 mice followed by 1-month CNO *i.p*. administration. ***Right bar charts***, serum PTH level, total serum calcium level, tibia trabecular bone mineral density (BMD), and femur cortical BMD from MicroCT analysis. **B**, ***upper left,*** immunohistofluorescence staining of CaMKII and GABA in the SFO of C57 mice. ***Lower left***, IHF staining of CaMKII colocalized with mCherry in the SFO of VGlut2-cre mice (n=3, scale bar, 100 μm). ***Upper right***, statistical analysis of GABA and CaMKII colocalization. ***Lower right***, statistical analysis of VGlut and CaMKII colocalization. **C**, *In situ* hybridization of GAD1/2 and VGlut2 mRNA in the SFO colocalized with cFos expression after *i.v.* PTH stimulation in C57 mice. Scale bar, 50 μm. **D**, Chemogenetic stimulation of GABAergic neurons in the SFO of C57 mice (n=6 mice). ***Left***, injection of AAV-GAD67-cre and AAV-DIO-hM3Dq/mCherry mixture into the SFO of C57 mice followed with 1-month CNO *i.p*. administration; ***Right bar charts***, serum PTH level, total serum calcium level, tibia trabecular BMD, and femur cortical BMD in MicroCT analysis. **E**, Chemogenetic

stimulation of glutamatergic neurons in the SFO of VGlut2-cre mice (n=5 mice). ***Left***, injection of AAV-DIO-hM3Dq/mCherry into the SFO of VGlut2-cre mice followed with 1- month CNO *i.p.* administration; ***Right bar charts***, serum PTH, total serum calcium level, tibia trabecular BMD, femur cortical BMD from MicroCT analysis. P analyzed by paired two-tailed t-test. All error bars and shaded areas show mean ± s.e.m. GABA, gamma-aminobutyric acid; CaMKII, calcium/calmodulin-dependent protein kinase II.

Figure 3. The function of PTH1R and PTH2R in the SFO.

A, PTH1R in the SFO colocalized with cFos expression after *i.v.* PTH stimulation Scale bar, 50 μm. **B**, PTH2R in the SFO colocalized with cFos expression after *i.v.* PTH stimulation (scale bar, 50 μm). **(c-e)** PTH and calcium tolerance tests in C57 mice after knockdown of PTH1R/PTH2R in the SFO (n=5-7). **C**, Injection of LV scaffold or LV-PTH1R-Cas9 or LV-PTH2R-Cas9 into the SFO of C57 mice. **D**, ***upper left***, serum PTH after *i.v.* injection of PTH; ***upper right***, serum calcium after *i.v.* injection of PTH; ***lower left***, serum PTH after *i.p.* injection of $CaCl_2$; ***lower right***, serum calcium after *i.p.* injection of $CaCl_2$ in control, SFO^{pth1r-} and SFO^{pth2r-} groups. The PTH and calcium level were quantified immediately before, and then 5, 15 and 30 min after PTH/$CaCl_2$ injection. **E**, Basic serum PTH and calcium level in control, SFO^{pth1r-} or SFO^{pth2r-} groups. **F**, GAD1/2 and VGlut2 mRNA expression colocalized with PTH1R and PTH2R staining of the SFO in C57 and PTH2R-$CreER^{T2}$ mice. **G**, Statistical analysis of colocalized cells (n=4 mice, scale bar, 50 μm). **H,** GAD1/2 and VGlut2 mRNA expression colocalized with PTH2R cells in the SFO of PTH2R-creERT2 mice. **I**, Statistical analysis of colocalized cells (n=4 mice, scale bar, 50 μm). Paired two-tailed t-test. All error bars and shaded areas show mean ± s.e.m.

Figure 4. PVN neurons regulate serum PTH level.

A, GAD1/2 and VGlut2 mRNA in the PVN colocalized with cFos staining after *i.v.* PTH stimulation. Scale bar, 100 μm. **B**, ***left and upper right*****,** colocalization of VGlut and CaMKII markers in the PVN of VGlut2-cre mice; ***lower right***, statistical analysis of the colocalized cells (n=3 mice). **C**, chemogenetic activation of CaMKII neurons in the PVN of C57 mice (n=5-6 mice). ***Left***, injection of AAV-CaMKII-hM3Dq/mCherry into the PVN of C57 mice followed with 1-month CNO *i.p*. administration. ***Right bar charts***, serum PTH, total serum calcium level, tibia trabecular bone mineral density (BMD), and femur cortical BMD from MicroCT analysis. **D**, Chemogenetic stimulation of VGlut neurons in the PVN of VGlut2-cre mice (n=5 mice). ***Left***, injection of AAV-DIO-hM3Dq/mCherry into the PVN of VGlut2-cre mice followed with 1-month CNO *i.p*. administration; ***Right bar charts***, serum PTH, total serum calcium level, tibia trabecular BMD, and femur cortical BMD from MicroCT analysis. **E,** 3D reconstruction of MicroCT analysis of tibia trabecular bone and femur cortical bone in C57 mice transfected with CaMKII-mCherry or CaMKII-hM3Dq-mCherry in the PVN and then given CNO for 1 month. **F**, 3D reconstruction of MicroCT result of tibia trabecular bone and femur cortical bone in VGlut2-cre mice transfected with DIO-hM3Dq-mCherry or DIO-mCherry in PVN and given CNO for 1 month. P analyzed by paired two-tailed t-test. All error bars and shaded areas show mean ± s.e.m.

Figure 5. SFO^{GABA} neurons send projections to the PVN.

A, ***Upper***, injection of AAV-GAD67-cre and AAV-DIO-mCherry mixture into the SFO of C57 mice; ***lower***, GABAergic neural projections observed from the SFO (***left***, scale

bar, 50 μm) to the PVN (***right***, scale bar, 100 μm). **B**, ***upper left***, injection of AAV9-DIO-TVA-RVG and then RV-dsRed into the PVN of VGlut2-cre mice; ***upper right***, RV tracing from PVN^{Glut} neurons (scale bar, 100 μm). ***Middle and lower***, colocalization of RV, CaMKII and GABA positive signals in SFO (scale bar, 50 μm). (**C-D**) Chemogenetic activation of SFO^{GABA}→PVN neural projections in C57 mice (n=6 mice). **C**, ***upper left***, injection of AAV-GAD67-cre into the SFO and AAV2retro-DIO-hM3Dq/mCherry into the PVN of C57 mice followed with 1-month CNO *i.p.* administration. ***Upper right,*** mCherry signals observed in the SFO indicating $GAD67^{+}$ neurons with axon terminals projected to PVN (scale bar, 50 μm). ***Lower***, serum PTH, total serum calcium level, tibia trabecular BMD, and femur cortical BMD in MicroCT analysis. **D**, 3D reconstruction of MicroCT analysis of tibia trabecular bone and femur cortical bone in C57 mice injected with GAD67-cre virus in the SFO and DIO-mCherry or DIO-hM3Dq-mCherry in the PVN and then given CNO for 1 month. P analyzed by paired two-tailed t-test. All error bars and shaded areas show mean ± s.e.m.

Figure 6. Peripheral innervation in parathyroid glands and regulation of PTH.

A, Innervation and location of tyrosine hydroxylase (TH^{+}) sympathetic nerves, $CD31^{+}$ capillaries and calcitonin gene-related peptide ($CGRP^{+}$) sensory nerves in mice parathyroid glands. Scale bar, 50 μm. **(B-C)**, Cholera toxin subunit B retrograde tracing from single side of rat parathyroid glands. **B**, CTB signals observed in the injection side and opposite side of sympathetic superior cervical ganglia (SCG). Scale bar, 500 μm. **C**, CTB signals observed in the injection side and opposite side of sympathetic inferior vagus ganglia. Scale bar, 500 μm. **(D-E)** Neural specific rabies virus (RV) tracing from mice parathyroid glands to the SCG and vagus ganglion. **D**, *in situ* RV (red) and helper

(green) expression in the parathyroid gland of PTH-cre mice. White arrow indicates colocalization of RV expression and helper expression signals. Scale bar, 50 μm. **E**, RV signals, TH expression in the SCG (*upper left*) and ChAT/CGRP expression in the vagus ganglion (*lower left*, *right*), white arrow indicates colocalization of RV signals and TH/ChAT/CGRP signals. Scale bar, 50 μm. **F**, ***up***, Serum PTH (***left***) and calcium (***right***) levels after *i.p.* injection of $CaCl_2$ in C57 mice with or without peripheral sympathetic nerve ablation with *i.p.* administration of 6-OHDA; ***lower***, serum PTH (***left***) and calcium (***right***) after *i.p.* injection of $CaCl_2$ in SD rats with or without sympathetic nerve ablation with local injection of 6-OHDA in the parathyroid gland. PTH and calcium were quantified immediately before, and then 5, 15 and 30 min after PTH/$CaCl_2$ injection (n=5-6). **G**, Schematic summarizing the mechanism underlying the neural regulation of PTH levels in the SFO and PVN. ChAT, choline acetyltranserase; 6-OHDA, 6-hydroxydopamine.

Figure S1. Poly-synaptic retrograde PRV labeling of specific rat brain nuclei

Pseudorabies virus (PRV) retrograde tracing from rat PTG to brain nuclei, including: the SFO, subfornical organ; OVLT, vascular organ of lamina terminalis; PVN, paraventricular thalamic nucleus; MPO, medial preoptic nucleus; SCh, suprachiasmatic nucleus; AP, area postrema; SolM, nucleus of the solitary tract, medial part; NTS, nucleus of the solitary tract; MnPO, median preoptic nucleus; MPOL, medial preoptic nucleus, lateral part; IO, inferior olive; LH, lateral hypothalamic area; VMH, ventromedial hypothalamic nucleus; Arc, arcuate nucleus (n=3 mice).

Figure S2. cFos expression in the mouse brain after peripheral *i.v.* PTH stimulation.

A, Immunoflourescent cFos signals (green) were observed in specific brain nuclei including: the PVA, paraventricular thalamic nucleus, anterior part; MPOL, medial preoptic nucleus, lateral part; SCh, suprachiasmatic nucleus; SO, supraoptic nucleus; SFO, subfornical organ; Arc, arcuate hypothalamic nucleus; PVN, paraventricular thalamic nucleus; BLA, basolateral amygdaloid nucleus, anteriorpart; AP, area postrema; 10N, dorsal motor nucleus of vagus; EW, Edinger-Westphal nucleus. **B**, Locations of PTH-responding nuclei and relative cFos expression density (n=3 mice).

Figure S3. PTH-biotin binding to specific brain nuclei after peripheral *i.v.* administration.

A, PTH-Biotin binds to different nuclei in the C57 mouse brain, including: the SCh, suprachiasmatic nucleus; SO, supraoptic nucleus; Sol, solitary tract; LGP, lateral globus pallidus; mfb, medial forebrain bundle, SFO, subfornical organ; Pe, periventricular hypothalamic nucleus; pv, periventricular fiber system; AP, area postrema. **B**, PTH binding nuclei location and the signal density (n=3 mice).

Figure S4. Bone analysis following chemogenetic regulation of SFO neurons

A, Bone analysis after stimulation of SFO^{CaMKII} neurons. ***Left***, 3D reconstruction of MicroCT analysis of tibia trabecular and femur cortical bones in hM3Dq and mCherry groups. ***Right bar charts***, tibia trabecular percent bone volume (BV/TV), trabecular thickness (Tb.Th), trabecular number (Tb.N), trabecular separation (Tb.Sp) assessed by MicroCT (n=9 mice). **B**, Bone analysis after stimulation of SFO^{GABA} neurons. ***Left***, 3D reconstruction of MicroCT analysis of tibia trabecular and femur cortical bones in hM3Dq and mCherry groups. ***Right bar charts***, BV/TV, Tb.Th, Tb.N and Tb.Sp assessed by MicroCT analysis (n=6 mice). **c**, Bone analysis after stimulating SFO^{VGlut2}

neurons. ***left***, 3D reconstruction of MicroCT analysis of tibia trabecular and femur cortical bones in hM3Dq and mCherry groups of VGlut2-cre mice. ***Right bar charts***, BV/TV, Tb.Th, Tb.N and Tb.Sp assessed by MicroCT analysis (n=5 mice). P analyzed by paired two-tailed t-test. All error bars and shaded areas show mean ± s.e.m.

Figure S5. Neural Projections of SFO^{CaMKII} neurons in the mouse brain.

A, SFO^{CaMKII} neurons labeled with AAV-CaMKII-mCherry project terminals into brain nuclei, including: the LSD, lateral septal nucleus, dorsal part; MPO, medial preoptic nucleus; PVN, paraventricular thalamic nucleus; HDB, nucleus of the horizontal limb of the diagonal band; SFi, septofimbrial nucleus; SHi, septohippocampal nucleus; SL, semilunar nucleus; DP, dorsal peduncular cortex; MCLH, magnocellular nucleus of the lateral hypothalamus; MCPO, magnocellular preoptic nucleus; MnPO, median preoptic nucleus; OVLT, vascular organ of lamina terminalis ;SuML, supramammillary nucleus, lateral part; SuMM, supramammillary nucleus, medial part;. **B**, Locations of brain nuclei receiving SFO^{CaMKII} neuronal projections (n=9 mice).

Figure S6. Behavioral and fluid-consumption tests of mice after knockdown of PTH1R/PTH2R expression in the SFO.

A, Behavioral tests in c57 mice after knockdown of PTH1R/PTH2R expression in the SFO. ***Left,*** time spent in the center during open field test. ***Middle***, open-arm time during elevated plus maze. ***Right***, immobility time during tail suspension test (n=5-6 mice for each chart). **B**. Fluid consumption (water or 0.3M NaCl) tests in c57 mice after knockdown of PTH1R/PTH2R expression in the SFO. ***Left,*** consumption of water and NaCl, ***right***, total fluid consumption (n=5-6 mice). P analyzed using paired two-tailed t-tests. All error bars and shaded areas show mean ± s.e.m.

Figure S7. Chemogenetic stimulation of SFO^{PTH2R} neurons in PTH2R- CreERT2 mice.

A, Immunofluorescent staining against cre recombinase and PTH2R in SFO and median eminence (ME) of PTH2R-CreER^{T2} mice. Scale bar, 50 μm. **B**, PTH2R neurons labeled by injecting AAV-DIO-mCherry into the SFO of PTH2R-CreER^{T2} mice and colocalization with NeuN (green). Scale bar, 50 μm. (**C-E**) Chemogenetic activation of PTH2R neurons in the SFO of PTH2R- CreER^{T2} mice (n=8 mice, scale bar, 50 μm). **C**, Injection of AAV-DIO-hM3Dq/mCherry into the SFO of PTH2R- CreER^{T2} mice followed with 1-month CNO *i.p.* administration. **D**, Serum PTH, total calcium level, tibia trabecular bone mineral density (BMD), and femur cortical BMD from MicroCT analysis. **E,** Behavioral tests after activation of SFO^{PTH2R} neurons. Time in center during open field test, open-arm time during elevated plus maze, immobility time during tail suspension test and fluid consumption quantity (water or 0.3M NaCl) were analyzed (n=8 mice). P analyzed using paired two-tailed t-test. All error bars and shaded areas show mean ± s.e.m.

Figure S8. Bone analysis after chemogenetic stimulation of PVN neurons.

A，The tibia trabecular percent bone volume (BV/TV), trabecular thickness (Tb.Th), trabecular numbers (Tb.N), trabecular separation (Tb.Sp) assessed by MicroCT analysis after chemogenetic stimulation of PVN^{CaMKII} neurons for 1 month in C57 mice (n=5-6 mice). **B,** Tibia trabecular BV/TV, Tb.Th, Tb.N and Tb.Sp assessed by MicroCT analysis after chemogenetic stimulation of PVN^{VGlut} neurons in VGlut2-cre mice (n=5 mice). P analyzed using paired two-tailed t-test. All error bars and shaded areas show mean ± s.e.m.

Figure S9. Bone analysis and behavioral tests following stimulation of the SFO^{GAD}→PVN neural circuit

A, Tibia trabecular percent bone volume (BV/TV), trabecular thickness (Tb.Th), trabecular numbers (Tb.N), trabecular separation (Tb.Sp) assessed by MicroCT analysis after chemogenetic stimulation of SFO^{GAD}→PVN for 1 month in C57 mice (n=6 mice).

B，Behavioral tests after activation of the SFO^{GAD}→PVN neural circuit. Time in center during an open field test, open-arm time during the elevated plus maze test, immobility time during tail suspension test, and fluid consumption (water or 0.3 M NaCl) were compared amongst groups (n=6 mice/group). P analyzed using paired two-tailed t-test. All error bars and shaded areas show mean ± s.e.m.

STAR METHODS

KEY RESOURCES TABLE

REAGENT or RESOURCE	SOURCE	IDENTIFIER
Antibodies		
goat anti-Biotin	Sigma	Cat#F6762, RRID:AB_259706
rabbit anti-calcium sensing receptor	abcam	Cat#ab62214, RRID:AB_942204
mouse anti-CaMKII	abcam	Cat#ab22609, RRID:AB_447192
goat anti-CD31	R&D	Cat#AF3628, RRID:AB_2161028
rabbit anti-cFos	Cell signaling	Cat#2250, RRID:AB_2247211
mouse anti-CGRP	abcam	Cat#ab81887, RRID:AB_1658411
rabbit anti-ChAT	abcam	Cat#ab6168, RRID:AB_2244866
mouse anti cre-recombinase	Millipore	Cat#mab3120, RRID:AB_2085748
rabbit anti-GABA	Sigma	Cat#A2052, RRID:AB_477652
chicken anti-GFP	abcam	Cat#ab13970, RRID:AB_300798
mouse anti-TH	Sigma	Cat#T1299, RRID:AB_477560

Goat anti rabbit Alexa Fluor 488	Jackson laboratory	Cat#111-547-003, RRID: AB_2338058
Goat anti rabbit Alexa Fluor 594	Jackson laboratory	Cat#111-587-003, RRID: AB_2338071
Goat anti mouse Alexa Fluor 488	Jackson laboratory	Cat#115-547-003, RRID: AB_2338869
Goat anti mouse Alexa Fluor, 594	Jackson laboratory	Cat#115-587-003, RRID: AB_2338900
Anti-Goat IgG-FITC	Sigma	Cat#F7367, RRID:AB_259726
Donkey anti rabbit Alexa Fluor 647	abcam	Cat#ab150075, RRID:AB_2752244
Donkey anti goat Alexa Fluor 647	abcam	Cat#ab150131, RRID:AB_2732857
Rabbit anti-PTH	LSbio	Cat#LS-C191152
rabbit anti-PTH1R	abcam	Cat#ab176393
rabbit anti-PTH2R	abcam	Cat#ab188760
chicken anti-NeuN	Millipore	Cat#ABN91, RRID:AB_11205760
Bacterial and Virus Strains		
PRV-CMV-EGFP	BrainVTA	P03001
DIO-EGFP-TVA-RVG	BrainVTA	N/A
RV-EnvA-ΔG-dsRed	BrainVTA	R01001
AAV9-CaMKII-mCherry	BCBDI, SIAT	N/A
AAV9-CaMKII-hM3Dq-mCherry	BCBDI, SIAT	N/A
AAV9-DIO-mCherry	BCBDI, SIAT	N/A
AAV9-DIO-hM3Dq-mCherry	BCBDI, SIAT	N/A
AAV9-GAD-cre	BCBDI, SIAT	N/A
AAV2retro-DIO-hM3Dq-mCherry	BCBDI, SIAT	N/A
AAV2retro-DIO-EYFP	BCBDI, SIAT	N/A
LV-PTH1R-Cas9	BCBDI, SIAT	N/A
LV-PTH2R-Cas9	BCBDI, SIAT	N/A
LV-empty	BCBDI, SIAT	N/A
Chemicals, Peptides, and Recombinant Proteins		
CTB- Alexa Fluor 488	Molecular Probes	Cat# C34775
Clozapine N-oxide	MCE	Cat# 34233-69-7
CaCl2	Sigma	Cat# C5670
hPTH (1-34)	MCE	Cat# 52232-67-4
EDTA-Na2	Sigma	Cat# E9884
hPTH (1-34)-Lys(Biotin)	AnaSpec	Cat# AS-23647
4′,6-diamidino-2-phenylindole, dihydrochloride	ThermoFisher	Cat# D1306
Critical Commercial Assays		
mouse PTH ELISA kits	LSBio	Cat# LS-5549
rat PTH ELISA kits	LSBio	Cat# LS-5548
Calcium colorimetric assay	Sigma	Cat# MAK022
6-hydroxydopamine hydrobromide	Sigma	Cat# H116
Experimental Models: Organisms/Strains		

PTH-cre mice	Jackson Laboratory	JAX: 005989
PTH2R- CreERT2 mice	GermPharmatech Co.	N/A
Vglut2-ires-Cre mice	Jackson LaboratorY	JAX: 016963
Oligonucleotides		
Gad1-RNA probe	BCBDI, SIAT	N/A
Gad2-RNA probe	BCBDI, SIAT	N/A
VGlut2-RNA probe	BCBDI, SIAT	N/A
Software and Algorithms		
GraphPad Prism		RRID:SCR_002798
ANY-maze video tracking software	Stoelting Co., IL,	N/A
Zen softwares	Zeiss	http://www.zeiss.com/corporate/en_de/global/home.html
pClamp 10	Axon instruments	https://www.moleculardevices.com/

CONTACT FOR REAGENT AND RESOURCE SHARING

Further information and requests for resources and reagents should be directed to and will be fulfilled by the Lead Contact, Fan Yang (fan.yang @siat.ac.cn).

EXPERIMENTAL MODEL AND SUBJECT DETAILS

Animals

C57/6J mice and SD rats (Beijing Vital River Laboratory Animal Technology Co) raised at the Shenzhen Institute of Advanced Technology, Chinese Academy of Science were used. VGlut2-ires-cre mice (Jackson Laboratory, 016863) and PTH-cre mice (Jackson Laboratory, 005989) were also used. PTH2R- CreER^{T2} mice were established and provided by GermPharmatech Co., Ltd. Only male mice/rats of 6-8 weeks-old were used in this study. All animals were housed under a Specific Pathogen Free (SPF) barrier environment according to the standard of GB14925-2010 Laboratory Animals Requirement of Housing and Facilities within a temperature-controlled room (20-26°C) with a 12-hour light/dark cycle (07:00 lights on, 19:00 lights off). Animals had free access to chow and water. All studies and experimental procedures were approved by

the Institutional Animal Care and Use Committee (IACUC) of the Shenzhen Institute of Advanced Technology, Chinese Academy of Science.

PTH2R- CreER^{T2} mice were generated based on C57/6J mice using the CRISPR-Cas9 technique by inserting a strand of cre recombinase with an estradiol receptor (ERT2) after the PTH2r promoter. Tamoxifen (75 mg/kg, i.p.) was administrated to the animal 5 days before experiments to initiate cre recombinase gene expression.

Retrograde neural tracing from parathyroid glands

Neural specific retrograde tracing was conducted with chlora toxin B (CTB- Alexa Fluor 488, 10 mg/mL, Molecular Probes®), modulated pseudorabies virus vector (PRV), modulated rabies virus vector (RV) and its adeno-associated virus (AAV) helper.

Non trans-synaptic retrograde tracing was conducted by CTB, which is absorbed by the neural terminals and can be transported to the neuronal soma. Monosynaptic retrograde tracing was performed with sequential use of AAV helper (DIO-EGFP-TVA-RVG) and modulated RV (RV-EnvA-ΔG-dsRed). The AAV helper was used for Cre-dependent expression of TVA, which directs the infection of RV and G proteins that reinstate the trans-synaptic infection. Poly-synaptic retrograde tracing was employed by pseudorabies virus (PRV-GFP), which infects the neural terminals of the injection site and is delivered to the soma and transfects to the next neuron through synaptic connection.

Helper AAV, RV and PRV (BrainVTA, Wuhan, China) were used with titers of 1.3E+12 PFU/mL, 5.0E+08 PFU/mL and 2.0E+09 PFU/mL, respectively. The retrograde tracers were injected into the parathyroid glands of mice and rats using a Hamilton®

microsyringe under anaesthesia (*i.p.* 100mg/kg sodium pentobarbital).

Virus injection and chemogenetic regulation of neurons

Adult mice of 6-8 weeks were anaesthetized (*i.p.* 100mg/kg sodium pentobarbital) and mounted on a stereotaxic frame (RWD Life Science, Shenzhen, China). Virus suspension (AAV9-CaMKII-mCherry, AAV9-CaMKII-hM3Dq-mCherry, AAV9-DIO-mCherry, AAV9-DIO-hM3Dq-mCherry, AAV9-GAD-cre, AAV2retro-DIO-hM3Dq-mCherry, AAV2retro-DIO-EYFP, LV-PTH1R-Cas9, LV-PTH2R-Cas9; LV-empty; 1.5-2.5E+12 PFU/mL) were loaded into a 5μl-Hamilton® syringe with 33-g needle, and 150 nL was injected with a speed of 100 nL/min by the targeting locations (SFO: -0.58, 0, -2.5; PVN: -0.8, ±0.5, -4.5) based on a stereotaxic atlas(Paxinos and Franklin, 2012). The surgical procedure was based on Lowery and Majewska(Lowery and Majewska, 2010). After surgery, animals were allowed to recover for at least 1 week before experiments. In chemogenetic studies, CNO (*i.p.* 1 mg/kg, MCE, 34233-69-7) was injected 3 weeks after virus expression, every 48 hours for 4 weeks prior to serum and bone collection and analysis.

PTH and calcium neural activation experiments and PTH binding assay

$CaCl_2$ (12 mM, Sigma, C5670), hPTH (1-34) (20 μg/mL, MCE, 52232-67-4), EDTA-Na_2 (12 mM, Sigma, E9884) and hPTH (1-34)-Lys(Biotin) (20 μg/mL, AnaSpec, AS-23647) were injected intravenously into C57 mice. Animals were returned to their home cage and transcardially perfused for tissue collection after 90-120 mins.

Immunohistofluorescence staining and *in situ* hybridization

Animals were anaesthetized with pentobarbital (100 mg/kg) and perfused intracardially

with PBS followed with 4% PFA. Tissue was collected and fixed in 4% PFA at 4 °C for 48 hours, and then dehydrated with 30% sucrose solution for 72 hours. Coronal sections of brain (35 μm) and parathyroid glands (PTG, 15 μm) were cut using a Cryostat microtome (Leica, CM1950) at -20 °C. The sections were washed twice with PBS, and blocked with blocking solutions (0.3% Tween20 in PBS with 5% goat normal serum or 5% bovine serum albumin) for 1 hour at room temperature, and then incubated overnight at 4 °C with appropriate primary antibodies diluted in 0.03% PBST. The primary antibodies used were: goat anti-Biotin (Sigma, F6762, 1:80), rabbit anti-calcium sensing receptor (abcam, ab62214, 1:500), mouse anti-CaMKII (abcam, ab22609, 1:500), goat anti-CD31 (R&D, AF3628, 1:20), rabbit anti-cFos (Cell signaling, #2250, 1:200), mouse anti-CGRP (abcam, 81887, 1:500), rabbit anti-ChAT (abcam, ab6168, 1:500), mouse anti cre-recombinase (Millipore, mab3120, 1:500), rabbit anti-GABA (Sigma, ab2052, 1:500), chicken anti-GFP (abcam, ab13970, 1:1000), rabbit anti-PTH (LSbio, LS-C191152, 1:500), rabbit anti-PTH1R (abcam, ab176393, 1:200), rabbit anti-PTH2R (abcam, ab188760, 1:200), mouse anti-TH (Sigma, T1299, 1:500), and chicken anti-NeuN (Millipore, ABN91, 1:500). Primary antibodies were washed three times with 0.1% PBST, and then replaced with appropriate secondary antibodies for 1 hour at room temperature and washed three times with 0.1% PBST. The secondary antibodies used were: Goat anti rabbit Alexa Fluor 488/594 (Jackson laboratory, 111-547-003/111-587-003, 1:200), Goat anti mouse Alexa Fluor 488/594 (Jackson laboratory, 115-547-003/115-587-003, 1:200), Anti-Goat IgG-FITC (Sigma, F7367, 1:400), Donkey anti rabbit Alexa Fluor 647 (abcam, ab150075, 1:1000), and Donkey anti goat Alexa Fluor 647 (abcam, ab150131, 1:1000). Sections were then incubated with 0.5 μg/ml 4′,6-diamidino-2-phenylindole, dihydrochloride (DAPI; ThermoFisher, D1306) for 1 min and Fluoromount-G (Southern Biotech, 0100-01).

In situ hybridization was performed to localize GABAergic and glutamatergic neurons with *Vglut2*, *Gad1* and *Gad2* probes. The procedure of *in situ* hybridization followed the procedure described by Kondoh et al.(Kondoh et al., 2016). Quantification of cell numbers labeled with different markers within different brain nuclei were calculated using 3 different slices from 3-4 different animals based on DAPI expression. The average of the three slices were taken and shown in graphs.

Biochemical analysis

Mouse and rat serum PTH levels were assessed with mouse and rat PTH ELISA kits (LSBio, LS-5549/LS-5548). Total serum calcium levels were obtained using a colorimetric assay (Sigma, MAK022). The results were read by a Nano Quant plate reader (Tecan, Infinite 200Pro).

Behavioral tests

Anxiety levels were assessed by an open-field test (OFT) and elevated plus-maze test (EPM). In the OFT, mice were placed in a corner of a square field of 80 × 80 cm, with walls of 80 cm and sufficient illumination. The elevated plus maze was elevated 50 cm from the ground, plus-shaped apparatus with two open and two enclosed arms (wall height 40 cm). The movement of animals from the entrance of the field/maze was recorded in an isolated room without interruption. The recording time for the OFT was 600 s and for the EPM it was 300 s. The time that each animal spent in different areas was assessed by analyzing software (Anymaze) to evaluate anxiety levels. Tail suspension tests (TST) were performed using a tail suspension cage (Bioseb, US). Mice were suspended by their tail with tape on the force transducer and the recording time

was 360 s. The time spent immobile was analyzed using Anymaze within the Bioseb's suspension cage.

Fluid consumption tests were performed in cages with two bottles. Animals were single housed to acclimatize to two bottles of water for 3 days and then completely water restricted for 12 hours before the test. Two bottles of water and 300 mM NaCl solution was provided to the animals during the test. Bottles were weighed every 2 hours within the first 6 hours during which the animals were free to access the fluids. The position of the bottles was changed after the first 1 hour to avoid position preference.

PTH and calcium tolerance test

Animal blood samples were collected before and after administration of human PTH (1-34) (*i.v.* 2 μg for mice) or $CaCl_2$ (*s.c.* 3 μM for mice, 15 μM for rats) and serum PTH and calcium levels were assessed before, 5 min, 15 min and 30 min after administration. Blood was collected from the retro-orbital sinus of mice and from the jugular vein from rats under anesthesia with isoflurane.

Micro-CT scanning and analysis

Mice femora and tibiae were collected and immersed in 4% paraformaldehyde before micro-CT scanning (SkyScan, model 1076). Scanning was performed using the following settings: isotropic voxel 11.53 μm, voltage 48 kV, current 179 μA, and exposure time of 1800 ms. Three-dimensional (3D) reconstruction was conducted using SkyScan NRecon software (version 1.6.8.0, SkyScan) with a voxel size of 8.66 μm. Datasets were reoriented using DataViewer (version 1.4.4.0, SkyScan), while the calculation of morphological parameters were carried out with the CTAn software

(version 1.13.2.1, SkyScan). The 3D reconstructed models were displayed by CTVol software (version 2.2.3.0, SkyScan).

Trabecular bone was selected 0.1-0.9 mm distal to the proximal tibia growth plate. The region of interest (ROI) was selected from 2D images slice-by-slice by hand to exclude the cortical area and then binarization of the images with a global thresholding of gray level (70-255) as mineralized tissue, according to the tuning 3D reconstruction of the mineralized tissue. A Gaussian filter (radius=1) was used for 3D reconstruction. Quantitative analysis involved all bone areas within the ROI of the 3D images. Morphometric parameters included total volume (TV, m^3), bone volume (BV, m^3), bone fraction (BV/TV, m^3), trabecular thickness (Tb. Th, 1/mm), trabecular number (Tb. N, 1/mm), and trabecular separation (Tb. SP, mm). In addition, the bone mineral density (BMD, g/cm^3) of the whole trabecular bone was calibrated using the attenuation coefficient of two hydroxyapatite phantoms with defined mineral densities of 0.25 and 0.75 g/cm^3.

Cortical bone was selected 6.5-7.2 mm proximal to the distal femur growth plate. The region of interest (ROI) was selected from 2D images with a threshold (85-255) as mineralized tissue. A Gaussian filter (radius=1) was used for 3D reconstruction. Quantitative analysis involved all bone areas within the ROI of the 3D images. Morphometric parameters included BV and BMD (within selected bone area).

Electrophysiology

Animals were sacrificed under deep anesthesia and brains removed and placed in ice-cold cutting solution for 1 min (110 mM Choline Chloride, 2.5 mM KCl, 0.5 mM $CaCl_2$,

7 mM $MgCl_2$, 1.3 mM NaH_2PO_4, 1.3 mM Na-ascorbate, 0.6 mM Na-pyruvate, 20 mM glucose and 2.5 $NaHCO_3$, 290-310 mOsm/kg, saturated with 95% O_2 and 5% CO_2). Coronal slices (300 μm) were cut using a vibrating microtome (VT1000, Leica), and then allowed to recover for 30 min at 37 °C in artificial cerebral spinal fluid (aCSF, 125 mM NaCl, 2.5 mM KCl, 2 mM $CaCl_2$, 1.3 mM $MgCl_2$, 1.3 mM NaH_2PO_4, 1.3 mM Na-ascorbate, 0.6 mM Na-pyruvate, 5 mM glucose, 5mM sucrose and 2.5 mM $NaHCO_3$, 300-310 mOsm/kg, saturated with 95% O_2 and 5% CO_2). After recovery, brain slices were transferred to a recording chamber and perfused with 2 ml/min aCSF. Patch pipettes were pulled from borosilicate glass (PG10150-4, World Precision Instruments) and filled with intrapipette solution (35 mM K-gluconate, 10 mM HEPES, 0.2 mM EGTA, 5 mM QX-314, 2 mM Mg-ATP, 0.1 mM Na-GTP, 8 mM NaCl, at 280~290 mOsm/kg and adjusted to pH 7.3 with KOH). Whole-cell patch clamp recording of SFO neurons was performed at room temperature (22–25 °C) with a Multiclamp 700B amplifier connected to a Digidata 1440A interface (Axon Instruments). Data were sampled at 10 kHz and analyzed with pClamp10 (Molecular Devices) or MATLAB (MathWorks).

Ablation of the sympathetic nerves in the PTG

Sympathetic nervous ablation was performed with 6-hydroxydopamine hydrobromide (6-OHDA, Sigma, H116). Universal ablation of sympathetic nerves was performed in mice by *i.p.* injection of 15 mg/kg 6-OHDA. *In situ* ablation of sympathetic nerves in parathyroid glands was performed by direct injection of 1 μL of 6-OHDA into the parathyroid glands. Calcium tolerance tests were performed 24 hours after 6-OHDA administration.

Statistical analysis

In all studies, results were presented as mean ± standard error of the mean (SEM) with n= number of individual animals. Statistical analysis was performed using unpaired Student's t-test for control and treatment comparisons, wherever appropriate, using the statistical program Prism version 7 (GraphPad Software, San Diego, CA, USA). A difference was accepted as statistically significant when probability (P) values were less than 0.05.

Reference

ANDERSON, J. W., WASHBURN, D. L. & FERGUSON, A. V. 2000. Intrinsic osmosensitivity of subfornical organ neurons. *Neuroscience,* 100**,** 539-47.

BAIN, V. E., GORDON, J., O'NEIL, J. D., RAMOS, I., RICHIE, E. R. & MANLEY, N. R. 2016. Tissue-specific roles for sonic hedgehog signaling in establishing thymus and parathyroid organ fate. *Development,* 143**,** 4027-4037.

BALDOCK, P. A., LIN, S., ZHANG, L., KARL, T., SHI, Y., DRIESSLER, F., ZENGIN, A., HORMER, B., LEE, N. J., WONG, I., LIN, E., ENRIQUEZ, R. F., STEHRER, B., DURING, M. J., YULYANINGSIH, E., ZOLOTUKHIN, S., RUOHONEN, S. T., SAVONTAUS, E., SAINSBURY, A. & HERZOG, H. 2014. Neuropeptide Y Attenuates Stress-Induced Bone Loss Through Suppression of Noradrenaline Circuits. *journal of bone and mineral research,* 29**,** 2238-2249.

CANARIO, A. V., ROTLLANT, J., FUENTES, J., GUERREIRO, P. M., RITA TEODOSIO, H., POWER, D. M. & CLARK, M. S. 2006. Novel bioactive parathyroid hormone and related peptides in teleost fish. *FEBS Lett,* 580**,** 291-9.

CHEN, H., SHOUMURA, S. & EMURA, S. 2005. Nerve fibres in the parathyroid gland of the golden hamster (Mesocricetus auratus): immunohistochemical and ultrastructural investigations. *Anat Histol Embryol,* 34**,** 34-7.

CHOU, F. F., CHEN, J. B., HSIEH, K. C. & LIOU, C. W. 2008. Cognitive changes after parathyroidectomy in patients with secondary hyperparathyroidism. *Surgery,* 143**,** 526-32.

DIMITROV, E. L., KUO, J., KOHNO, K. & USDIN, T. B. 2013. Neuropathic and inflammatory pain are modulated by tuberoinfundibular peptide of 39 residues. *Proc Natl Acad Sci U S A,* 110**,** 13156-61.

DOBOLYI, A., DIMITROV, E., PALKOVITS, M. & USDIN, T. B. 2012. The neuroendocrine functions of the parathyroid hormone 2 receptor. *Front Endocrinol (Lausanne),* 3**,** 121.

DOBOLYI, A., PALKOVITS, M. & USDIN, T. B. 2010. The TIP39-PTH2 receptor system: unique peptidergic cell groups in the brainstem and their interactions with central regulatory mechanisms. *Prog Neurobiol,* 90**,** 29-59.

DRIESSEN, M., WETTERLING, T., WEDEL, T. & PREUSS, R. 1995. Secondary hyperparathyroidism and depression in chronic renal failure. *Nephron,* 70**,** 334-9.

EGAWA, C. & KAMEDA, Y. 1995. Innervation of the chicken parathyroid glands: immunohistochemical study with the TuJ1, galanin, VIP, substance P, CGRP and tyrosine hydroxylase antibodies. *Anat Embryol (Berl),* 191**,** 445-50.

FEGLEY, D., HOLMES, A., RIORDAN, T., FABER, C., WEISS, J., MA, S., BATKAI, S., PACHER, P., DOBOLYI, A. & MURPHY, A. 2008. Increased fear - and stress - related anxiety - like behavior in mice lacking tuberoinfundibular peptide of 39 residues. *Genes, Brain and Behavior,* 7**,** 933-942.

FISCHER, J. A., BLUM, J. W. & BINSWANGER, U. 1973. Acute parathyroid hormone response to epinephrine in vivo. *J Clin Invest,* 52**,** 2434-40.

HOTTA, H., ONDA, A., SUZUKI, H., MILLIKEN, P. & SRIDHAR, A. 2017a. Modulation of calcitonin, parathyroid hormone, and thyroid hormone secretion by electrical stimulation of sympathetic and parasympathetic nerves in anesthetized rats. *Frontiers in neuroscience,* 11**,** 375.

HOTTA, H., ONDA, A., SUZUKI, H., MILLIKEN, P. & SRIDHAR, A. 2017b. Modulation of Calcitonin, Parathyroid Hormone, and Thyroid Hormone Secretion by Electrical Stimulation of Sympathetic and Parasympathetic Nerves in Anesthetized Rats. *Front Neurosci,* 11**,** 375.

JENDRYKA, M., PALCHAUDHURI, M., URSU, D., VAN DER VEEN, B., LISS, B., KÄTZEL, D., NISSEN, W. & PEKCEC, A. 2019. Pharmacokinetic and pharmacodynamic actions of clozapine-N-oxide, clozapine, and compound 21 in DREADD-based chemogenetics in mice. *Scientific reports,* 9**,** 1-14.

JOBORN, C., HETTA, J., NIKLASSON, F., RASTAD, J., WIDE, L., ÅGREN, H., ÅKERSTRÖM, G. & LJUNGHALL, S. 1991. Cerebrospinal fluid calcium, parathyroid hormone, and monoamine and purine metabolites and the blood-brain barrier function in primary hyperparathyroidism. *Psychoneuroendocrinology,* 16**,** 311-322.

JOBORN, C., HETTA, J., PALMER, M., AKERSTROM, G. & LJUNGHALL, S. 1986. Psychiatric symptomatology in patients with primary hyperparathyroidism. *Ups J Med Sci,* 91**,** 77-87.

KAWABE, T., CHITRAVANSHI, V. C., KAWABE, K. & SAPRU, H. N. 2008. Cardiovascular function of a glutamatergic projection from the hypothalamic paraventricular nucleus to the nucleus tractus solitarius in the rat. *Neuroscience,* 153**,** 605-617.

KOLLARS, J., ZARROUG, A. E., VAN HEERDEN, J., LTEIF, A., STAVLO, P., SUAREZ, L., MOIR, C., ISHITANI, M. & RODEBERG, D. 2005. Primary hyperparathyroidism in pediatric patients. *Pediatrics,* 115**,** 974-80.

KONDOH, K., LU, Z., YE, X., OLSON, D. P., LOWELL, B. B. & BUCK, L. B. 2016. A specific area of olfactory cortex involved in stress hormone responses to predator odours. *Nature,* 532**,** 103-106.

LIU, J. Y., PEINE, B. S., MLAVER, E., PATEL, S. G., WEBER, C. J., SAUNDERS, N. D., POFAHL, W. E. & SHARMA, J. 2020. Neuropsychologic changes in primary hyperparathyroidism after parathyroidectomy from a dual-institution prospective study. *Surgery*.

LIU, Y., IBRAHIM, A. S., TAY, B. H., RICHARDSON, S. J., BELL, J., WALKER, T. I., BRENNER, S., VENKATESH, B. & DANKS, J. A. 2010. Parathyroid hormone gene family in a cartilaginous fish, the elephant shark (Callorhinchus milii). *J Bone Miner Res,* 25**,** 2613-23.

LOWERY, R. L. & MAJEWSKA, A. K. 2010. Intracranial injection of adeno-associated viral vectors. *JoVE (Journal of Visualized Experiments)***,** e2140.

LUTS, L., BERGENFELZ, A., ALUMETS, J., LUTS, A. & SUNDLER, F. 1996. VIP- and PACAP-containing nerve fibers in human parathyroid glands and adenomas: comparison of innervation pattern with animal species. *Ann N Y Acad Sci,* 805**,** 661-5.

MATSUDA, T., HIYAMA, T. Y., NIIMURA, F., MATSUSAKA, T., FUKAMIZU, A., KOBAYASHI, K., KOBAYASHI, K. & NODA, M. 2017. Distinct neural mechanisms for the control of thirst and salt appetite in the subfornical organ. *Nature neuroscience,* 20**,** 230.

MCKINLEY, M. J., MCALLEN, R. M., DAVERN, P., GILES, M. E., PENSCHOW, J., SUNN, N., USCHAKOV, A. & OLDFIELD, B. J. 2003. The sensory circumventricular organs of the mammalian brain. *Adv Anat Embryol Cell Biol,* 172**,** III-XII, 1-122, back cover.

MORTIMER, S. T., HANLEY, D. A. & STELL, W. K. 1990. Immunohistochemical identification of calcitonin gene-related peptide and substance P in nerves of the bovine parathyroid gland. *Cell Tissue Res,* 261**,** 339-45.

MUNGER, J. S. & SHEPPARD, D. 2011. Cross talk among TGF-β signaling pathways, integrins, and the extracellular matrix. *Cold Spring Harbor perspectives in biology,* 3**,** a005017.

NATION, H. L., NICOLEAU, M., KINSMAN, B. J., BROWNING, K. N. & STOCKER, S. D. 2016. DREADD-induced activation of subfornical organ neurons stimulates thirst and salt appetite. *Journal of neurophysiology,* 115**,** 3123-3129.

OKA, Y., YE, M. & ZUKER, C. S. 2015. Thirst driving and suppressing signals encoded by distinct neural populations in the brain. *Nature,* 520**,** 349.

PAXINOS, G. & FRANKLIN, K. B. J. 2012. *Paxinos and Franklin's the Mouse Brain in Stereotaxic Coordinates*.

POLICENI, B. A., SMOKER, W. R. & REEDE, D. L. Anatomy and embryology of the thyroid and parathyroid glands. Seminars in Ultrasound, CT and MRI, 2012. Elsevier, 104-114.

ROMAN, S. A., SOSA, J. A., PIETRZAK, R. H., SNYDER, P. J., THOMAS, D. C., UDELSMAN, R. & MAYES, L. 2011. The effects of serum calcium and parathyroid hormone changes on psychological and cognitive function in patients undergoing parathyroidectomy for primary hyperparathyroidism. *Ann Surg,* 253**,** 131-7.

ROMEO, H. E., GONZALEZ SOLVEYRA, C., VACAS, M. I., ROSENSTEIN, R. E., BARONTINI, M. & CARDINALI, D. P. 1986. Origins of the sympathetic projections to rat thyroid and parathyroid glands. *J Auton Nerv Syst,* 17**,** 63-70.

SHI, Z., PELLETIER, N. E., WONG, J., LI, B., SDRULLA, A. D., MADDEN, C. J., MARKS, D. L. & BROOKS, V. L. 2020. Leptin increases sympathetic nerve activity via induction of its own receptor in the paraventricular nucleus. *Elife,* 9**,** e55357.

SHOUMURA, S., IWASAKI, Y., ISHIZAKI, N., EMURA, S., HAYASHI, K., YAMAHIRA, T.,

SHOUMURA, K. & ISONO, H. 1983. Origin of autonomic nerve fibers innervating the parathyroid gland in the rabbit. *Acta Anat (Basel),* 115**,** 289-95.
SUAREZ-BREGUA, P., CAL, L., CANESTRO, C. & ROTLLANT, J. 2017a. PTH Reloaded: A New Evolutionary Perspective. *Front Physiol,* 8**,** 776.
SUAREZ-BREGUA, P., SAXENA, A., BRONNER, M. E. & ROTLLANT, J. 2017b. Targeted Pth4-expressing cell ablation impairs skeletal mineralization in zebrafish. *PLoS One,* 12**,** e0186444.
SUAREZ-BREGUA, P., TORRES-NUÑEZ, E., SAXENA, A., GUERREIRO, P., BRAASCH, I., PROBER, D. A., MORAN, P., CERDA-REVERTER, J. M., DU, S. J. & ADRIO, F. 2016. Pth4, an ancient parathyroid hormone lost in eutherian mammals, reveals a new brain-to-bone signaling pathway. *The FASEB Journal,* 31**,** 569-583.
SWANSON, L. W. & SAWCHENKO, P. E. 1983. Hypothalamic integration: organization of the paraventricular and supraoptic nuclei. *Annu Rev Neurosci,* 6**,** 269-324.
TSUDA, M. C., YEUNG, H. M., KUO, J. & USDIN, T. B. 2015. Incubation of Fear Is Regulated by TIP39 Peptide Signaling in the Medial Nucleus of the Amygdala. *J Neurosci,* 35**,** 12152-61.
USDIN, T., HOARE, S., WANG, T., MEZEY, E. & KOWALAK, J. 1999. TIP39: a new neuropeptide and PTH2-receptor agonist from hypothalamus. *Nature neuroscience,* 2**,** 941.
VIVAS, L., CHIARAVIGLIO, E. & CARRER, H. F. 1990. Rat organum vasculosum laminae terminalis in vitro: responses to changes in sodium concentration. *Brain Res,* 519**,** 294-300.
WANG, T., PALKOVITS, M., RUSNAK, M., MEZEY, E. & USDIN, T. B. 2000. Distribution of parathyroid hormone-2 receptor-like immunoreactivity and messenger RNA in the rat nervous system. *Neuroscience,* 100**,** 629-49.
WEIN, M. N. & KRONENBERG, H. M. 2018. Regulation of Bone Remodeling by Parathyroid Hormone. *Cold Spring Harb Perspect Med,* 8.
ZIMMERMAN, C. A., LEIB, D. E. & KNIGHT, Z. A. 2017. Neural circuits underlying thirst and fluid homeostasis. *Nature Reviews Neuroscience,* 18**,** 459.
ZIMMERMAN, C. A., LIN, Y.-C., LEIB, D. E., GUO, L., HUEY, E. L., DALY, G. E., CHEN, Y. & KNIGHT, Z. A. 2016. Thirst neurons anticipate the homeostatic consequences of eating and drinking. *Nature,* 537**,** 680.

Figures

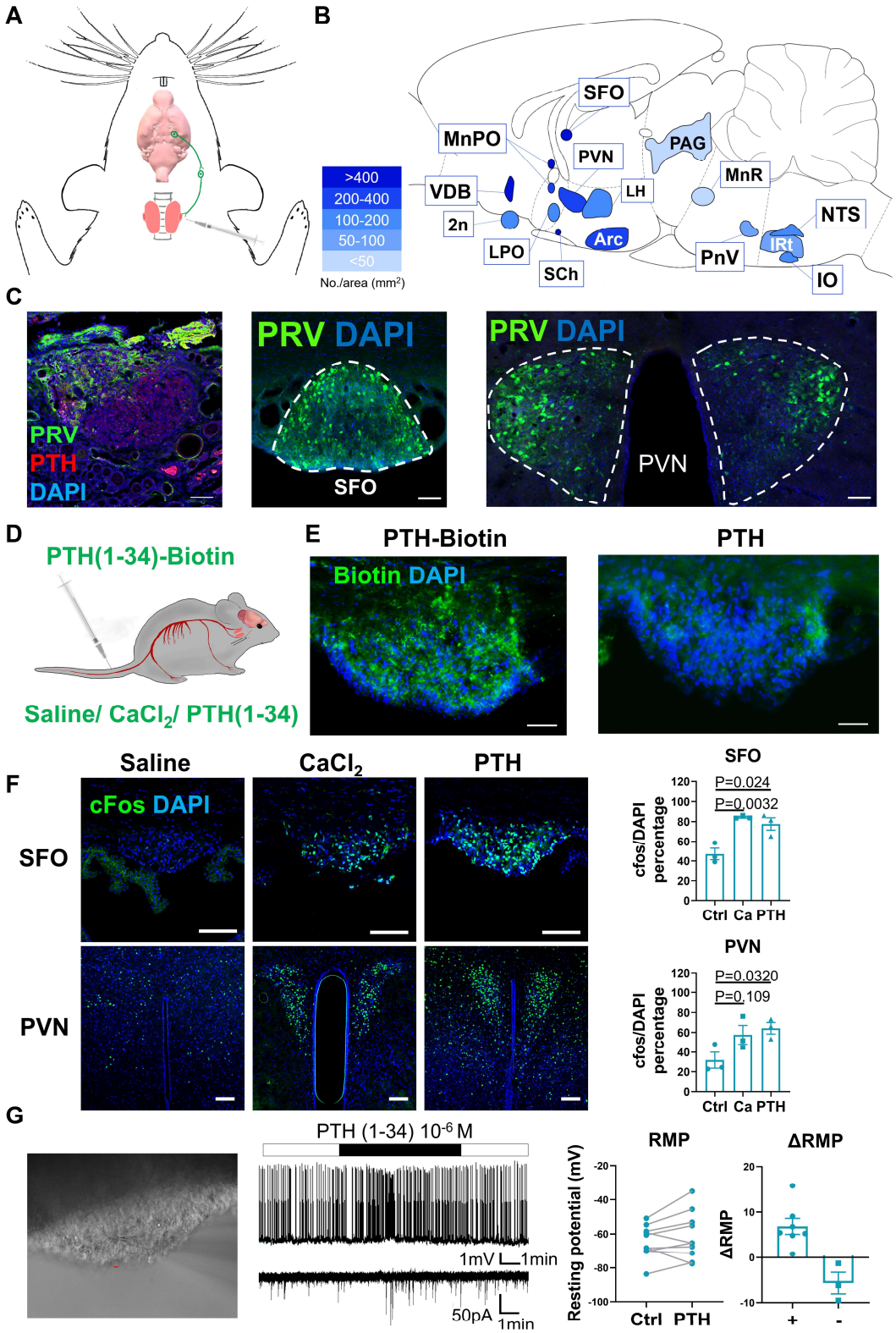

Figure 1. Parathyroid glands are connected to the SFO and PVN.

A, Schematic showing pseudorabies virus (PRV) infection of SD rat parathyroid gland

(PTG) and poly trans-synaptic connection to the central nervous system. **B**, PRV expression density in different rat brain areas after PRV neural tracing (No./mm^2, n=3). 2n, optic nerve; Arc, arcuate nucleus; IRT, intermediate reticular nucleus; IO, inferior olive; LH, lateral hypothalamic area; LPO, lateral preoptic area; MnPO, median preoptic nucleus; MnR, median raphe nucleus; NTS, nucleus tractus solitarius; PAG, periaqueductal gray; PnV, pontine reticular nucleus ventral part; PVN, paraventricular thalamic nucleus; SFO, subfornical organ; SCh, suprachiasmatic nucleus; VDB, nucleus of the vertical limb of the diagonal band. **C**, PRV positive signals in the PTG (***left,*** scale bar, 50 μm), SFO (***middle,*** scale bar, 100 μm) and PVN (***right,*** scale bar, 100 μm). **D**, Schematic showing peripheral administration of PTH (1-34), $CaCl_2$ and PTH-biotin. **E**, Peripherally administrated PTH-Biotin (green florescence) binds to the SFO; PTH without biotin was a negative control. Scale bar, 100 μm. **F**, cFos expression in the SFO (***upper left,*** scale bar, 100 μm) and PVN (***lower left,*** scale bar, 100 μm) after peripheral $CaCl_2$ or PTH administration. Quantification of cFos positive cells in the SFO and PVN (***right***, n=3). **G**, Electrophysiological recording of SFO cells with whole-cell patch (n=8). RPM, resting membrane potential, P analyzed by paired two-tailed t-test. All error bars and shaded areas show mean ± s.e.m.

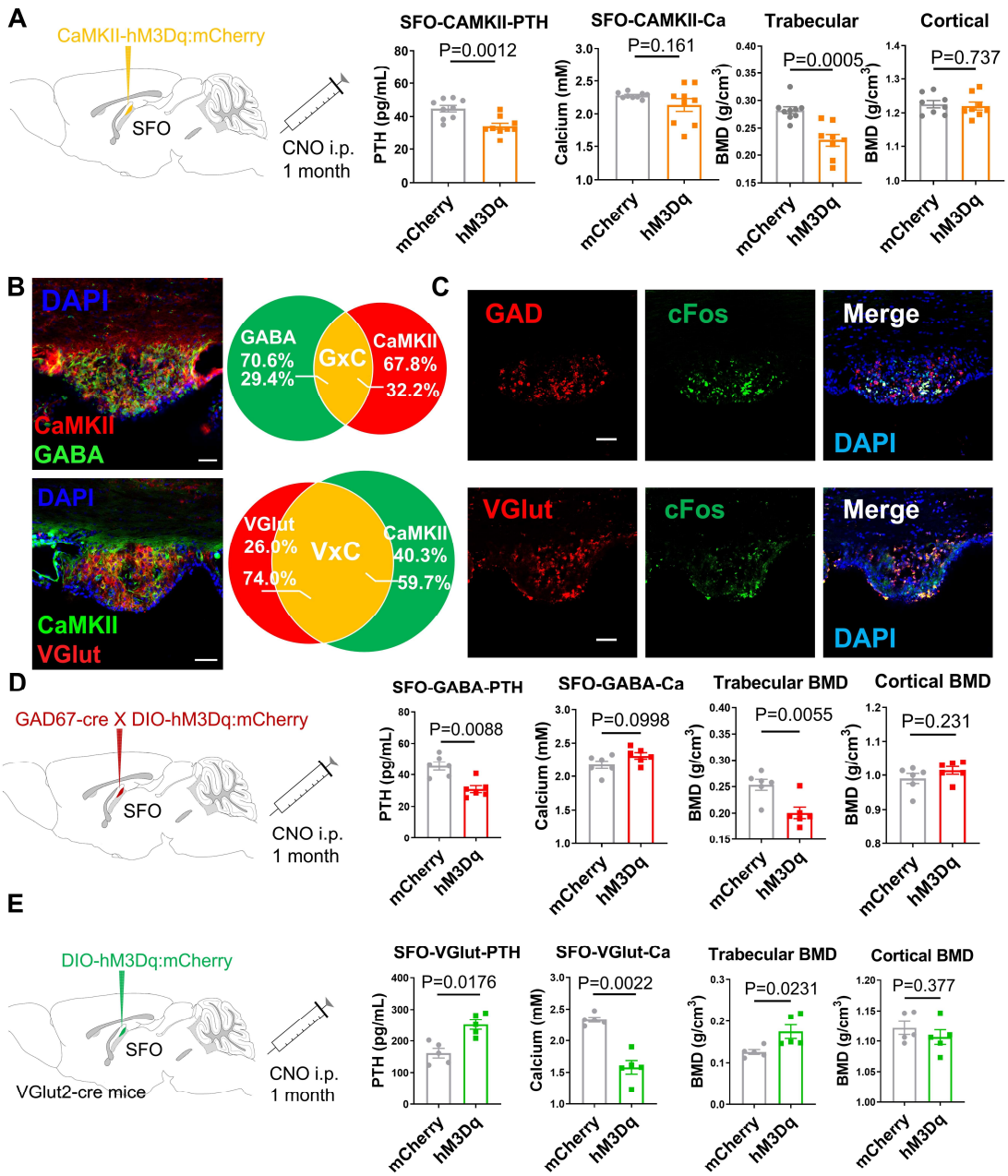

Figure 2. SFO neurons regulate serum PTH level.

A, Chemogenetic stimulation of CaMKII neurons in the SFO of C57 mice (n=9). ***Left***, injection of AAV-CaMKII-hM3Dq/mCherry into the SFO of C57 mice followed by 1-month CNO *i.p*. administration. ***Right bar charts***, serum PTH level, total serum calcium level, tibia trabecular bone mineral density (BMD), and femur cortical BMD from MicroCT analysis. **B**, ***upper left,*** immunohistofluorescence staining of CaMKII and GABA in the SFO of C57 mice. ***Lower left***, IHF staining of CaMKII colocalized with

mCherry in the SFO of VGlut2-cre mice (n=3, scale bar, 100 μm). ***Upper right***, statistical analysis of GABA and CaMKII colocalization. ***Lower right***, statistical analysis of VGlut and CaMKII colocalization. **C**, *In situ* hybridization of GAD1/2 and VGlut2 mRNA in the SFO colocalized with cFos expression after *i.v.* PTH stimulation in C57 mice. Scale bar, 50 μm. **D**, Chemogenetic stimulation of GABAergic neurons in the SFO of C57 mice (n=6 mice). ***Left***, injection of AAV-GAD67-cre and AAV-DIO-hM3Dq/mCherry mixture into the SFO of C57 mice followed with 1-month CNO *i.p.* administration; ***Right bar charts***, serum PTH level, total serum calcium level, tibia trabecular BMD, and femur cortical BMD in MicroCT analysis. **E**, Chemogenetic stimulation of glutamatergic neurons in the SFO of VGlut2-cre mice (n=5 mice). ***Left***, injection of AAV-DIO-hM3Dq/mCherry into the SFO of VGlut2-cre mice followed with 1- month CNO *i.p.* administration; ***Right bar charts***, serum PTH, total serum calcium level, tibia trabecular BMD, femur cortical BMD from MicroCT analysis. P analyzed by paired two-tailed t-test. All error bars and shaded areas show mean ± s.e.m. GABA, gamma-aminobutyric acid; CaMKII, calcium/calmodulin-dependent protein kinase II.

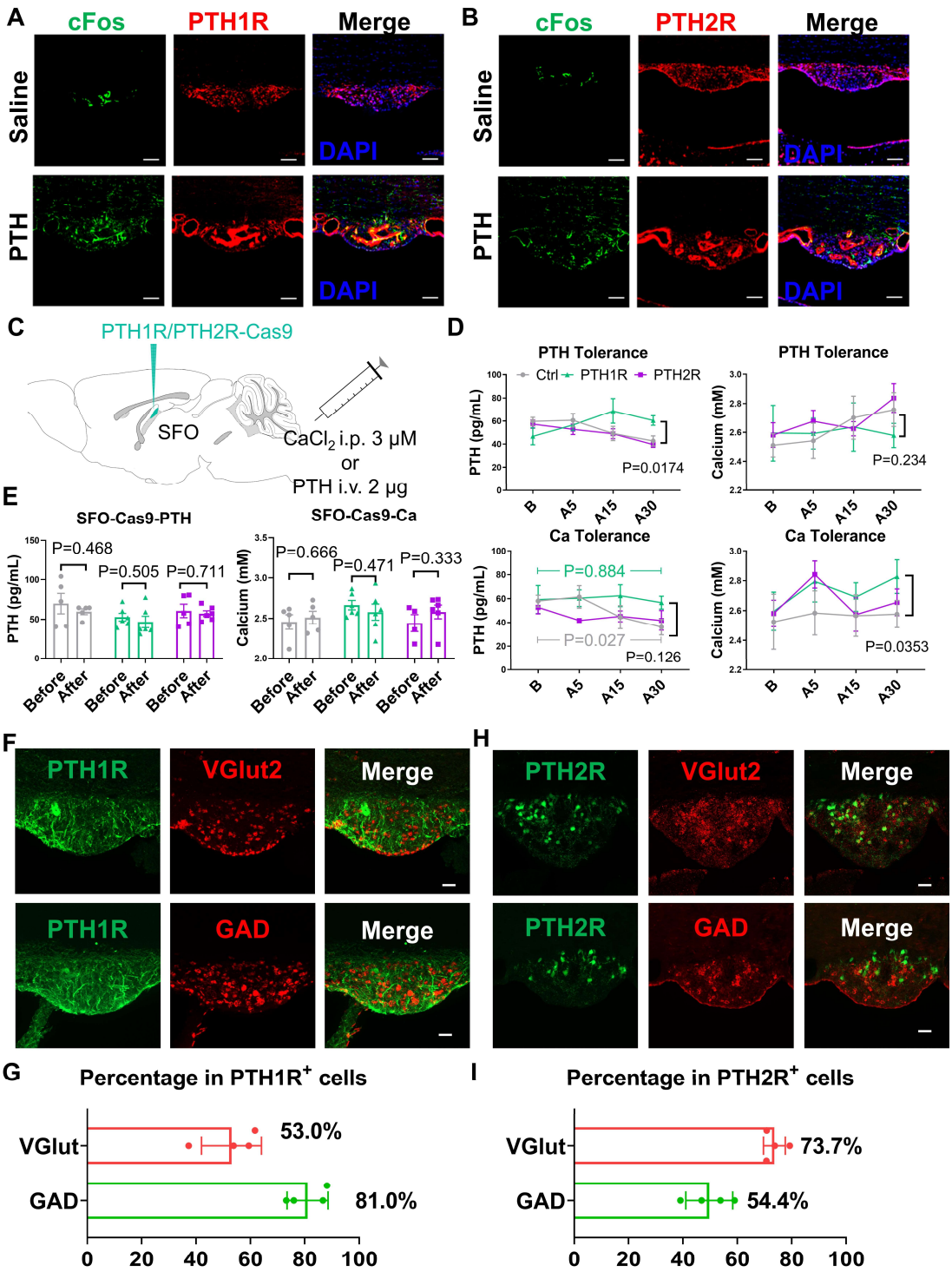

Figure 3. The function of PTH1R and PTH2R in the SFO.

A, PTH1R in the SFO colocalized with cFos expression after *i.v.* PTH stimulation Scale bar, 50 μm. **B**, PTH2R in the SFO colocalized with cFos expression after *i.v.* PTH stimulation (scale bar, 50 μm). **(c-e)** PTH and calcium tolerance tests in C57 mice after knockdown of PTH1R/PTH2R in the SFO (n=5-7). **C**, Injection of LV scaffold or LV-

PTH1R-Cas9 or LV-PTH2R-Cas9 into the SFO of C57 mice. **D**, ***upper left***, serum PTH after *i.v.* injection of PTH; ***upper right***, serum calcium after *i.v.* injection of PTH; ***lower left***, serum PTH after *i.p.* injection of $CaCl_2$; ***lower right***, serum calcium after *i.p.* injection of $CaCl_2$ in control, SFO^{pth1r-} and SFO^{pth2r-} groups. The PTH and calcium level were quantified immediately before, and then 5, 15 and 30 min after PTH/$CaCl_2$ injection. **E**, Basic serum PTH and calcium level in control, SFO^{pth1r-} or SFO^{pth2r-} groups. **F**, GAD1/2 and VGlut2 mRNA expression colocalized with PTH1R and PTH2R staining of the SFO in C57 and PTH2R-$CreER^{T2}$ mice. **G**, Statistical analysis of colocalized cells (n=4 mice, scale bar, 50 μm). **H,** GAD1/2 and VGlut2 mRNA expression colocalized with PTH2R cells in the SFO of PTH2R-creERT2 mice. **I**, Statistical analysis of colocalized cells (n=4 mice, scale bar, 50 μm). Paired two-tailed t-test. All error bars and shaded areas show mean ± s.e.m.

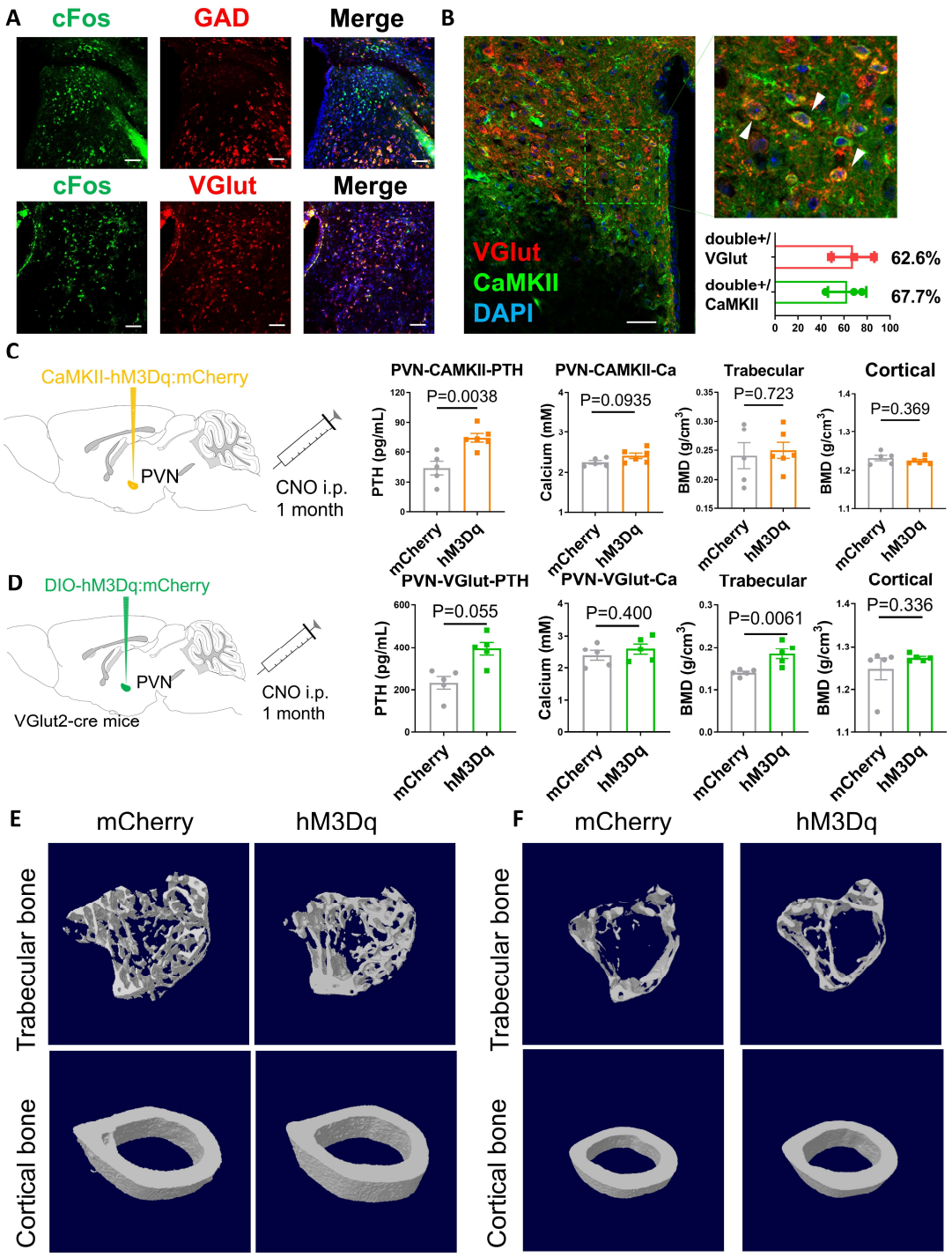

Figure 4. PVN neurons regulate serum PTH level.

A, GAD1/2 and VGlut2 mRNA in the PVN colocalized with cFos staining after *i.v.* PTH stimulation. Scale bar, 100 μm. **B**, ***left and upper right***, colocalization of VGlut and CaMKII markers in the PVN of VGlut2-cre mice; ***lower right***, statistical analysis of the colocalized cells (n=3 mice). **C**, chemogenetic activation of CaMKII neurons in

the PVN of C57 mice (n=5-6 mice). ***Left***, injection of AAV-CaMKII-hM3Dq/mCherry into the PVN of C57 mice followed with 1-month CNO *i.p*. administration. ***Right bar charts***, serum PTH, total serum calcium level, tibia trabecular bone mineral density (BMD), and femur cortical BMD from MicroCT analysis. **D**, Chemogenetic stimulation of VGlut neurons in the PVN of VGlut2-cre mice (n=5 mice). ***Left***, injection of AAV-DIO-hM3Dq/mCherry into the PVN of VGlut2-cre mice followed with 1-month CNO *i.p*. administration; ***Right bar charts***, serum PTH, total serum calcium level, tibia trabecular BMD, and femur cortical BMD from MicroCT analysis. **E,** 3D reconstruction of MicroCT analysis of tibia trabecular bone and femur cortical bone in C57 mice transfected with CaMKII-mCherry or CaMKII-hM3Dq-mCherry in the PVN and then given CNO for 1 month. **F**, 3D reconstruction of MicroCT result of tibia trabecular bone and femur cortical bone in VGlut2-cre mice transfected with DIO-hM3Dq-mCherry or DIO-mCherry in PVN and given CNO for 1 month. P analyzed by paired two-tailed t-test. All error bars and shaded areas show mean ± s.e.m.

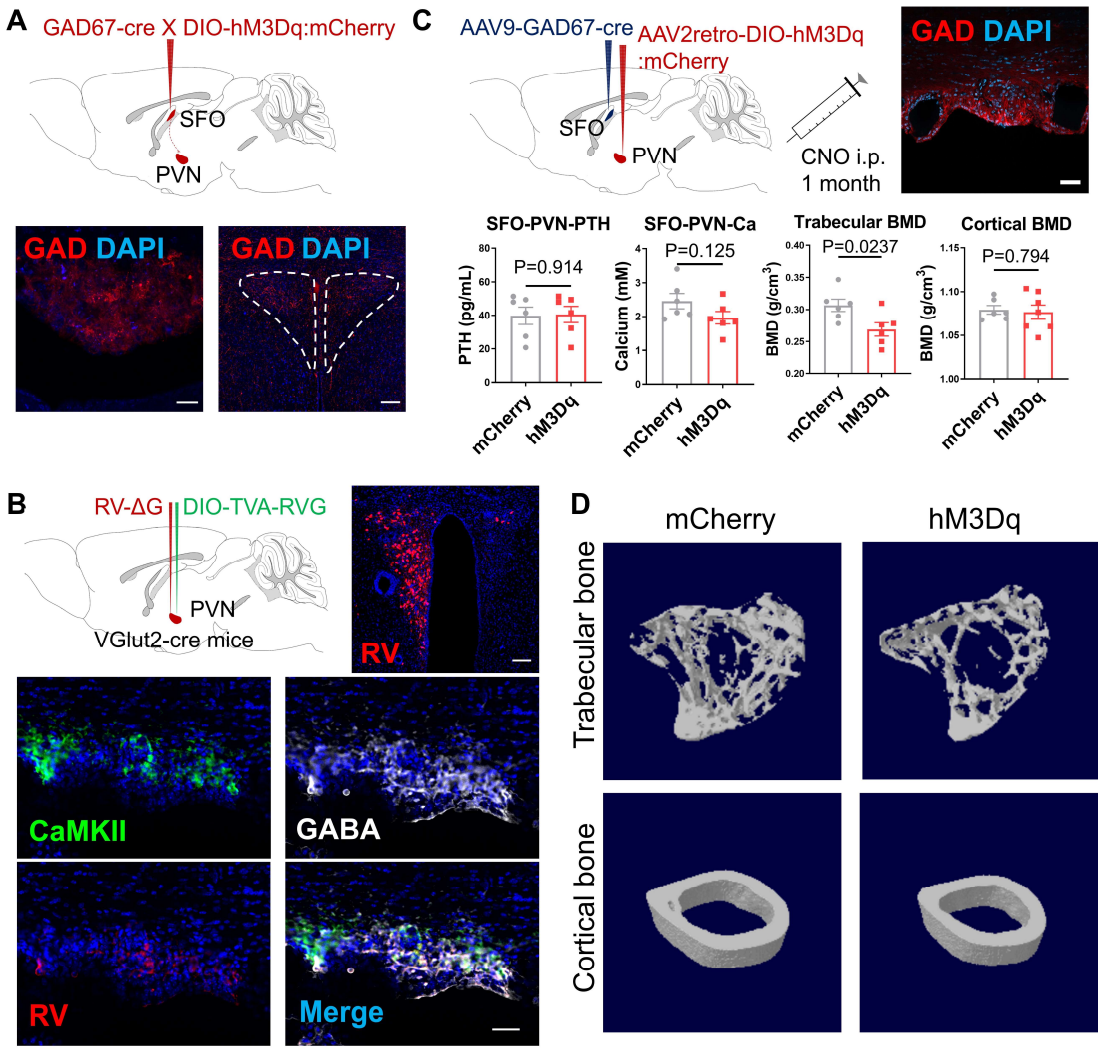

Figure 5. SFO^{GABA} neurons send projections to the PVN.

A, ***Upper***, injection of AAV-GAD67-cre and AAV-DIO-mCherry mixture into the SFO of C57 mice; ***lower***, GABAergic neural projections observed from the SFO (***left***, scale bar, 50 μm) to the PVN (***right***, scale bar, 100 μm). **B**, ***upper left***, injection of AAV9-DIO-TVA-RVG and then RV-dsRed into the PVN of VGlut2-cre mice; ***upper right***, RV tracing from PVN^{Glut} neurons (scale bar, 100 μm). ***Middle and lower***, colocalization of RV, CaMKII and GABA positive signals in SFO (scale bar, 50 μm). (**C-D**) Chemogenetic activation of SFO^{GABA}→PVN neural projections in C57 mice (n=6 mice). **C**, ***upper left***, injection of AAV-GAD67-cre into the SFO and AAV2retro-DIO-hM3Dq/mCherry into the PVN of C57 mice followed with 1-month CNO *i.p.*

administration. ***Upper right,*** mCherry signals observed in the SFO indicating GAD67^{+} neurons with axon terminals projected to PVN (scale bar, 50 μm). ***Lower***, serum PTH, total serum calcium level, tibia trabecular BMD, and femur cortical BMD in MicroCT analysis. **D**, 3D reconstruction of MicroCT analysis of tibia trabecular bone and femur
5 cortical bone in C57 mice injected with GAD67-cre virus in the SFO and DIO-mCherry or DIO-hM3Dq-mCherry in the PVN and then given CNO for 1 month. P analyzed by paired two-tailed t-test. All error bars and shaded areas show mean ± s.e.m.

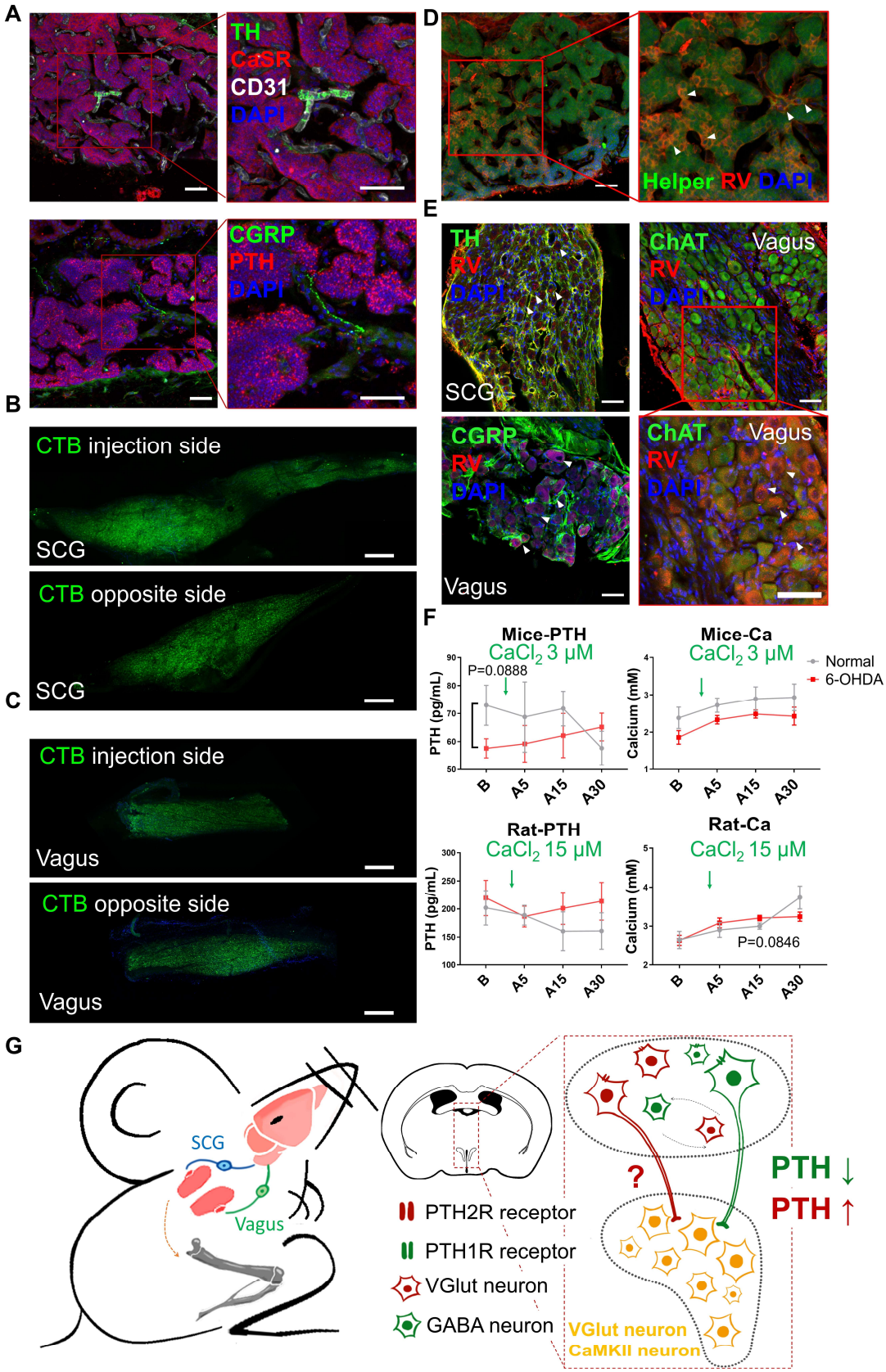

Figure 6. Peripheral innervation in parathyroid glands and regulation of PTH.

A, Innervation and location of tyrosine hydroxylase (TH^+) sympathetic nerves, $CD31^+$

capillaries and calcitonin gene-related peptide ($CGRP^+$) sensory nerves in mice parathyroid glands. Scale bar, 50 μm. **(B-C)**, Cholera toxin subunit B retrograde tracing from single side of rat parathyroid glands. **B**, CTB signals observed in the injection side and opposite side of sympathetic superior cervical ganglia (SCG). Scale bar, 500 μm. **C**, CTB signals observed in the injection side and opposite side of sympathetic inferior vagus ganglia. Scale bar, 500 μm. **(D-E)** Neural specific rabies virus (RV) tracing from mice parathyroid glands to the SCG and vagus ganglion. **D**, *in situ* RV (red) and helper (green) expression in the parathyroid gland of PTH-cre mice. White arrow indicates colocalization of RV expression and helper expression signals. Scale bar, 50 μm. **E**, RV signals, TH expression in the SCG (*upper left*) and ChAT/CGRP expression in the vagus ganglion (*lower left*, *right*), white arrow indicates colocalization of RV signals and TH/ChAT/CGRP signals. Scale bar, 50 μm. **F**, ***up***, Serum PTH (***left***) and calcium (***right***) levels after *i.p.* injection of $CaCl_2$ in C57 mice with or without peripheral sympathetic nerve ablation with *i.p.* administration of 6-OHDA; ***lower***, serum PTH (***left***) and calcium (***right***) after *i.p.* injection of $CaCl_2$ in SD rats with or without sympathetic nerve ablation with local injection of 6-OHDA in the parathyroid gland. PTH and calcium were quantified immediately before, and then 5, 15 and 30 min after PTH/$CaCl_2$ injection (n=5-6). **G**, Schematic summarizing the mechanism underlying the neural regulation of PTH levels in the SFO and PVN. ChAT, choline acetyltranserase; 6-OHDA, 6-hydroxydopamine

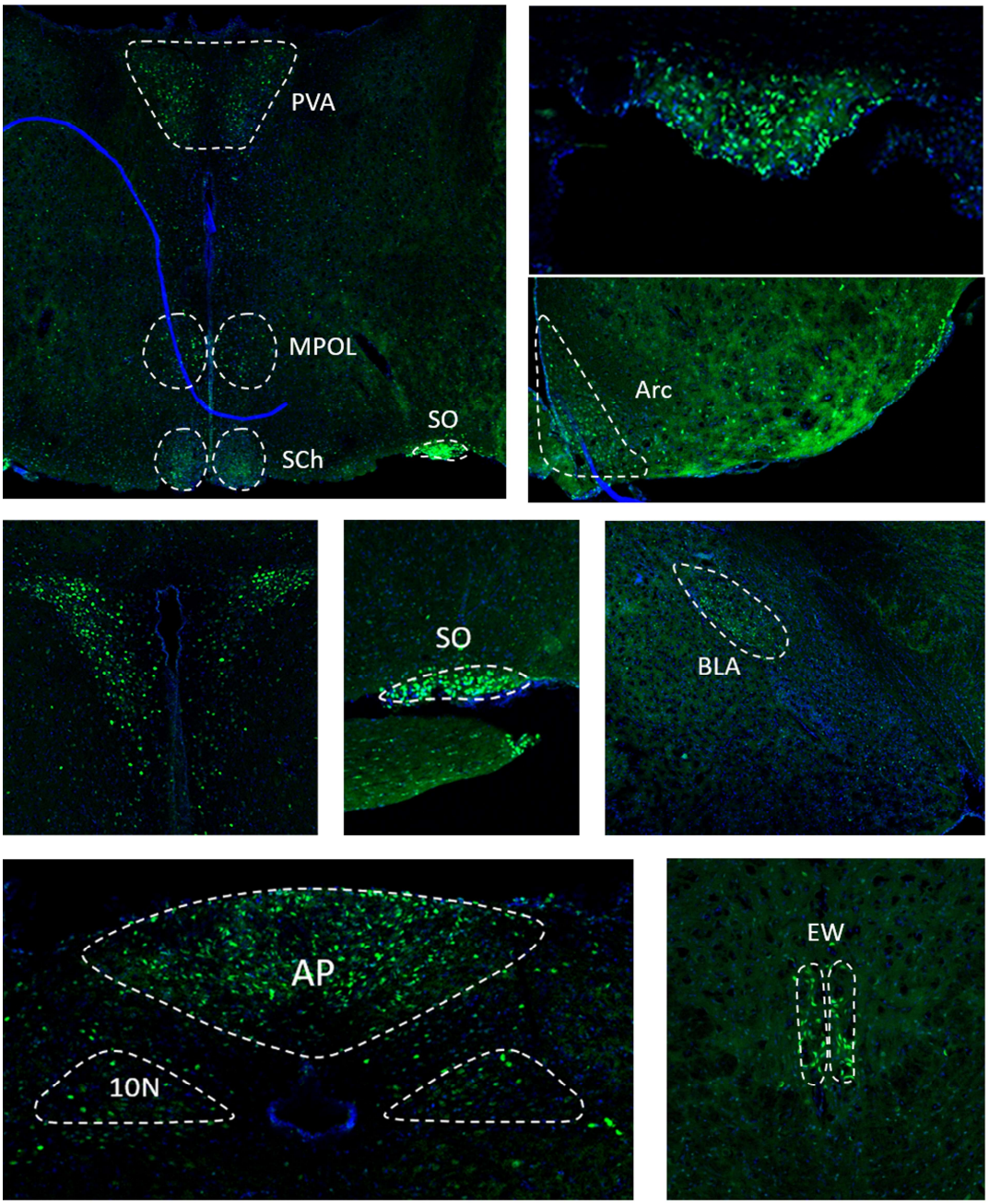

Supplementary figure 1. Poly-synaptic retrograde PRV labeling of specific rat brain nuclei

Pseudorabies virus (PRV) retrograde tracing from rat PTG to brain nuclei, including: the SFO, subfornical organ; OVLT, vascular organ of lamina terminalis; PVN, paraventricular thalamic nucleus; MPO, medial preoptic nucleus; SCh, suprachiasmatic nucleus; AP, area postrema; SolM, nucleus of the solitary tract, medial part; NTS, nucleus of the solitary tract; MnPO, median preoptic nucleus; MPOL, medial preoptic

nucleus, lateral part; IO, inferior olive; LH, lateral hypothalamic area; VMH, ventromedial hypothalamic nucleus; Arc, arcuate nucleus (n=3 mice).

A

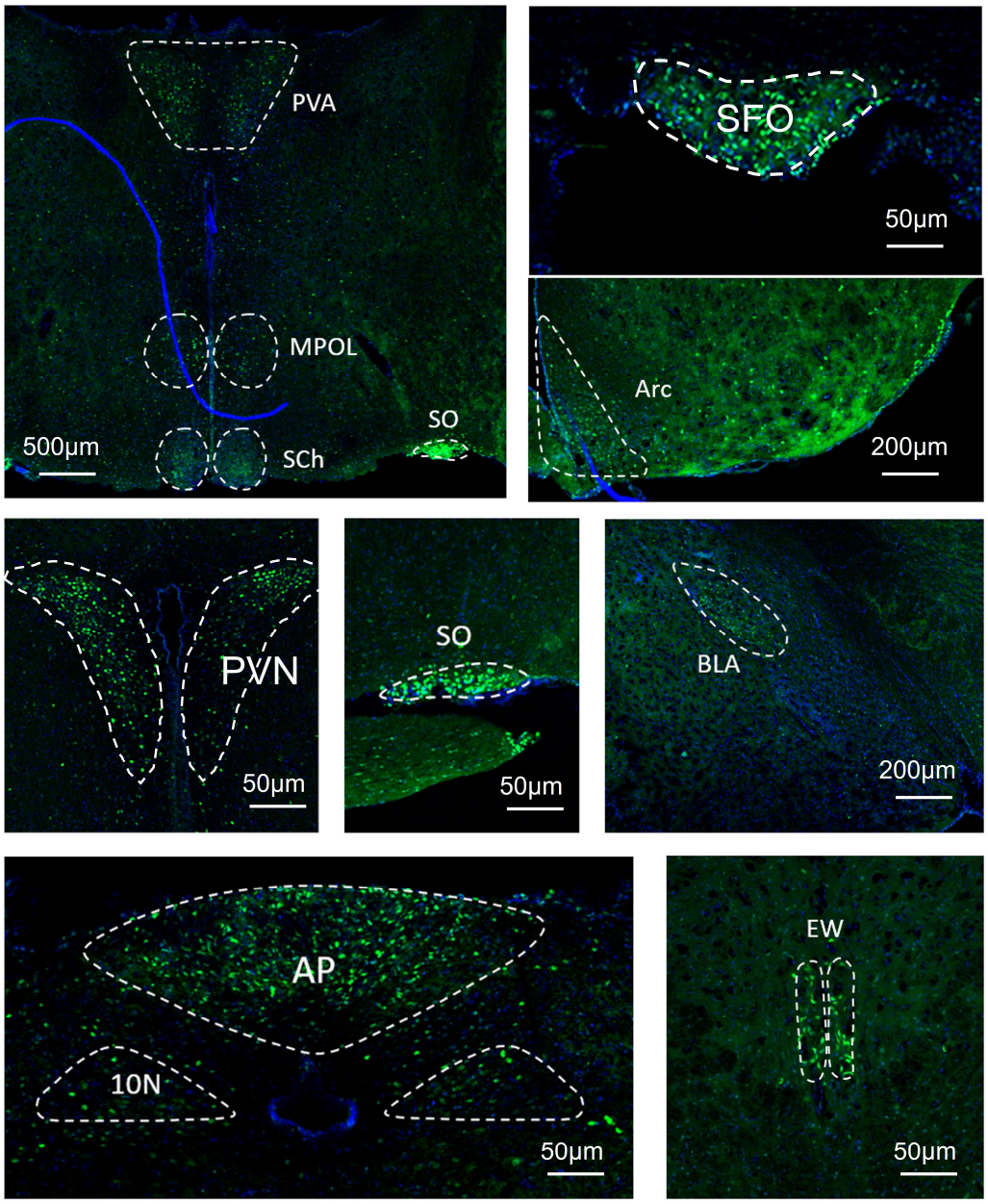
PVA
MPOL
SO
SCh
500μm
SFO
50μm
Arc
200μm
PVN
50μm
SO
50μm
BLA
200μm
AP
10N
50μm
EW
50μm

B

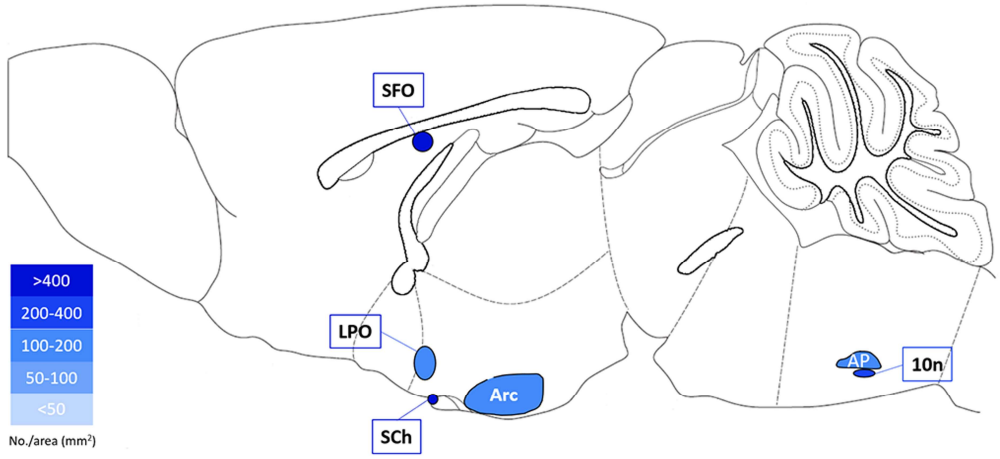
SFO
LPO
Arc
SCh
AP
10n
>400
200-400
100-200
50-100
<50
No./area (mm²)

Supplementary figure 2. cFos expression in the mouse brain after peripheral *i.v.* PTH stimulation.

A, Immunoflourescent cFos signals (green) were observed in specific brain nuclei including: the PVA, paraventricular thalamic nucleus, anterior part; MPOL, medial preoptic nucleus, lateral part; SCh, suprachiasmatic nucleus; SO, supraoptic nucleus; SFO, subfornical organ; Arc, arcuate hypothalamic nucleus; PVN, paraventricular thalamic nucleus; BLA, basolateral amygdaloid nucleus, anteriorpart; AP, area postrema; 10N, dorsal motor nucleus of vagus; EW, Edinger-Westphal nucleus. **B**, Locations of PTH-responding nuclei and relative cFos expression density (n=3 mice).

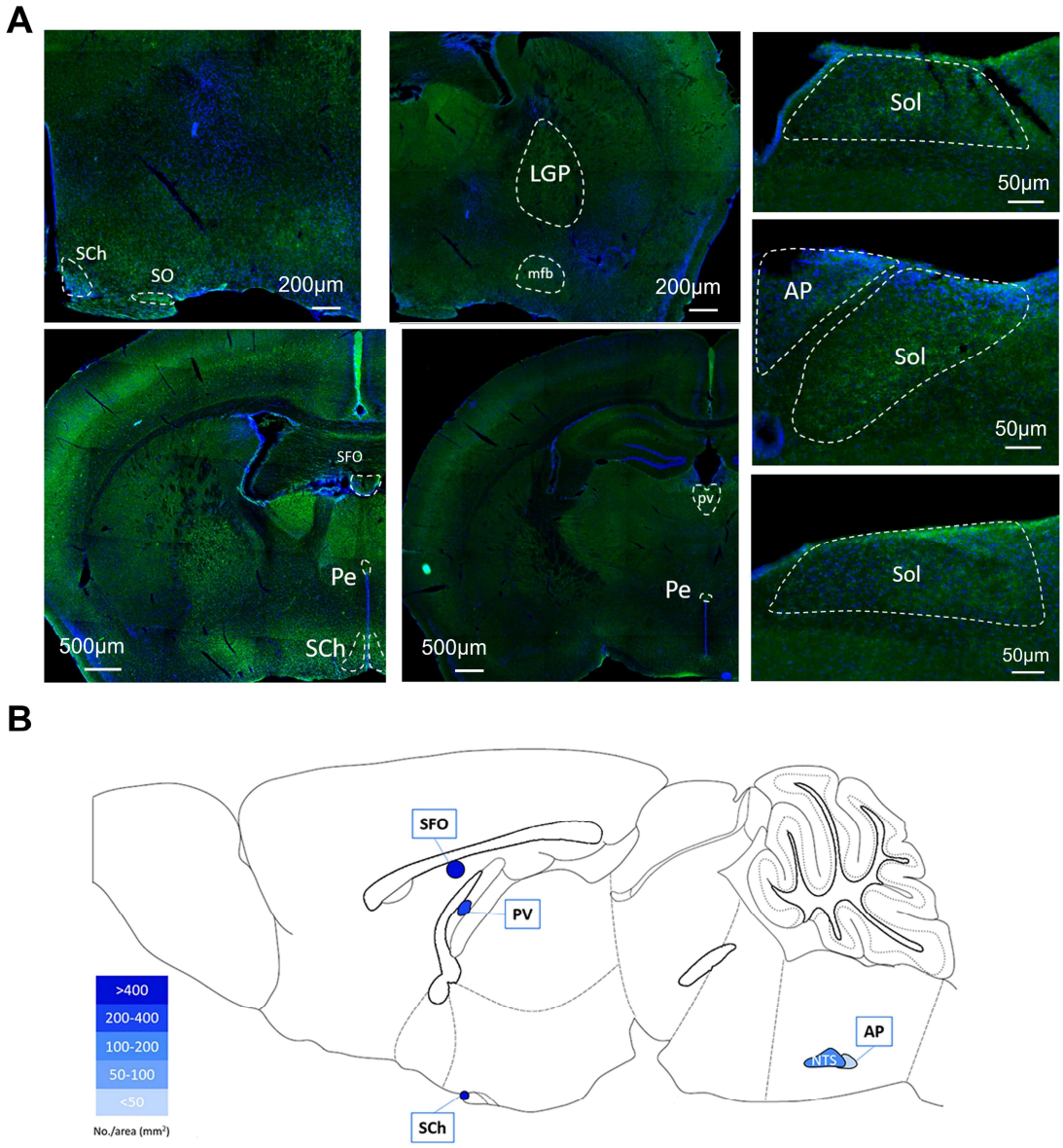

Supplementary figure 3. PTH-biotin binding to specific brain nuclei after peripheral *i.v.* administration.

A, PTH-Biotin binds to different nuclei in the C57 mouse brain, including: the SCh, suprachiasmatic nucleus; SO, supraoptic nucleus; Sol, solitary tract; LGP, lateral globus pallidus; mfb, medial forebrain bundle, SFO, subfornical organ; Pe, periventricular hypothalamic nucleus; pv, periventricular fiber system; AP, area postrema. **B**, PTH binding nuclei location and the signal density (n=3 mice).

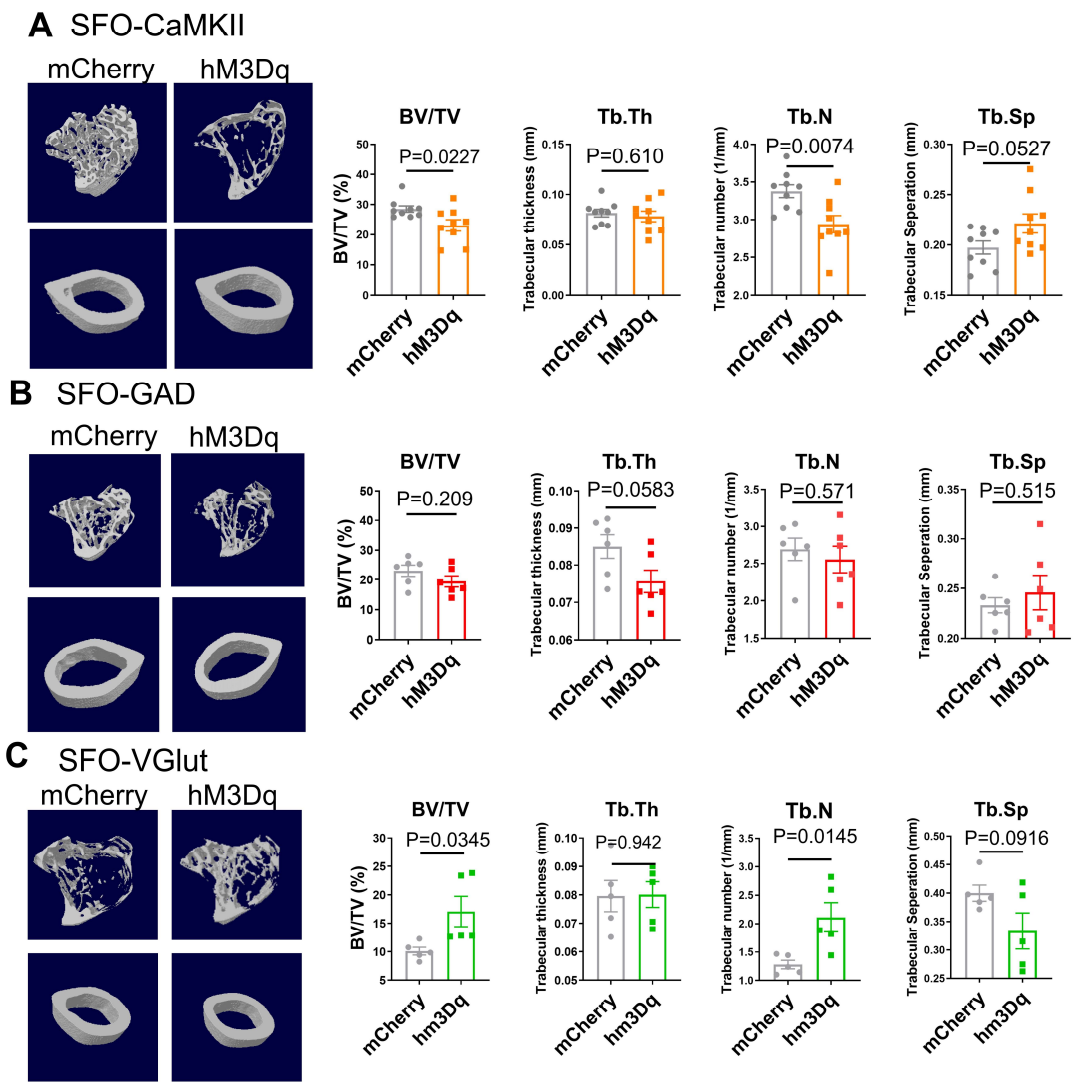

Supplementary figure 4. Bone analysis following chemogenetic regulation of SFO neurons

A, Bone analysis after stimulation of SFO^{CaMKII} neurons. ***Left***, 3D reconstruction of MicroCT analysis of tibia trabecular and femur cortical bones in hM3Dq and mCherry groups. ***Right bar charts***, tibia trabecular percent bone volume (BV/TV), trabecular thickness (Tb.Th), trabecular number (Tb.N), trabecular separation (Tb.Sp) assessed by MicroCT (n=9 mice). **B**, Bone analysis after stimulation of SFO^{GABA} neurons. ***Left***, 3D reconstruction of MicroCT analysis of tibia trabecular and femur cortical bones in hM3Dq and mCherry groups. ***Right bar charts***, BV/TV, Tb.Th, Tb.N and Tb.Sp assessed by MicroCT analysis (n=6 mice). **c**, Bone analysis after stimulating SFO^{VGlut2}

neurons. ***left***, 3D reconstruction of MicroCT analysis of tibia trabecular and femur cortical bones in hM3Dq and mCherry groups of VGlut2-cre mice. ***Right bar charts***, BV/TV, Tb.Th, Tb.N and Tb.Sp assessed by MicroCT analysis (n=5 mice). P analyzed by paired two-tailed t-test. All error bars and shaded areas show mean ± s.e.m.

5

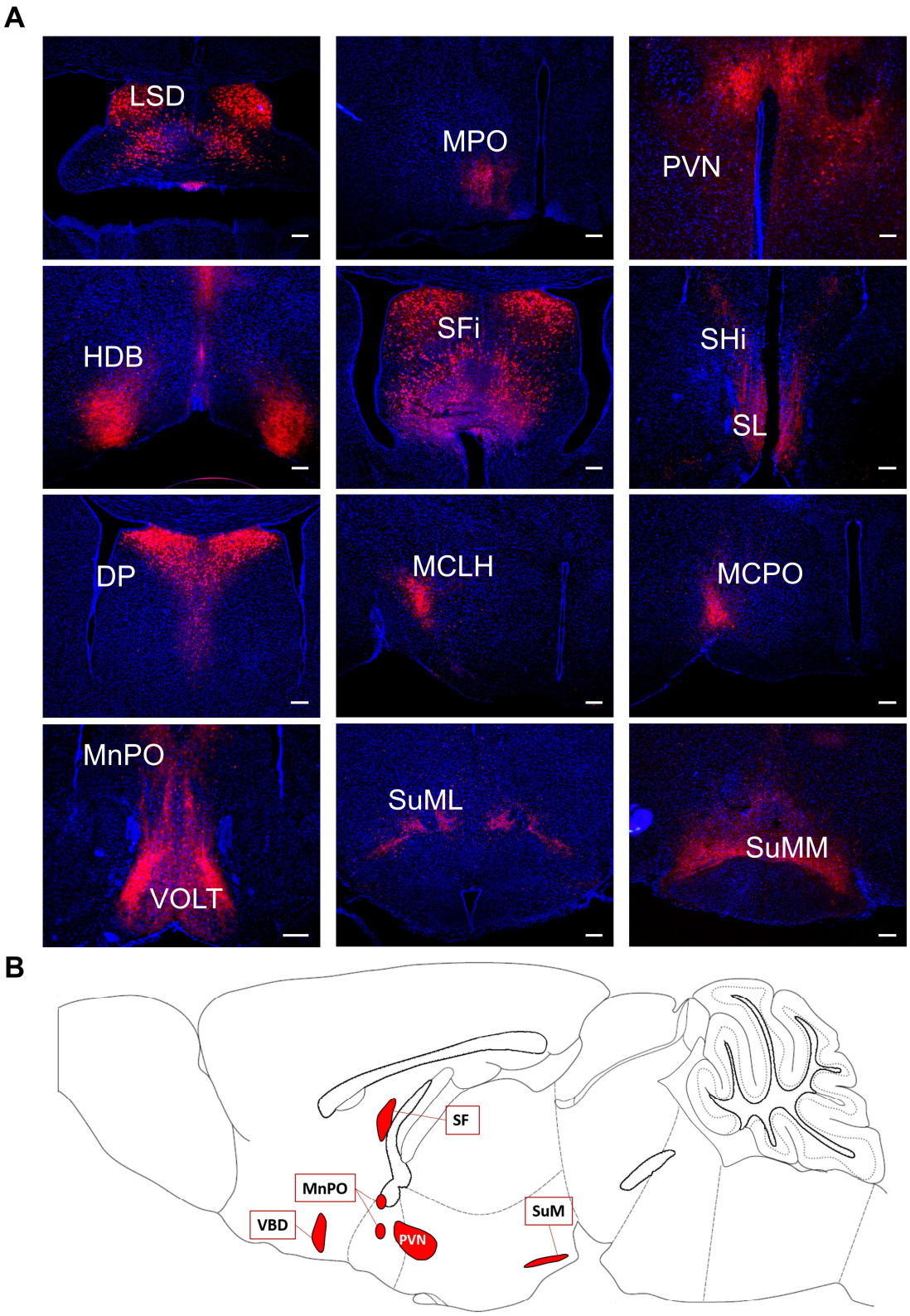

Supplementary figure 5. Neural Projections of SFO^{CaMKII} neurons in the mouse brain.

A, SFO^{CaMKII} neurons labeled with AAV-CaMKII-mCherry project terminals into brain

nuclei, including: the LSD, lateral septal nucleus, dorsal part; MPO, medial preoptic nucleus; PVN, paraventricular thalamic nucleus; HDB, nucleus of the horizontal limb of the diagonal band; SFi, septofimbrial nucleus; SHi, septohippocampal nucleus; SL, semilunar nucleus; DP, dorsal peduncular cortex; MCLH, magnocellular nucleus of the lateral hypothalamus; MCPO, magnocellular preoptic nucleus; MnPO, median preoptic nucleus; OVLT, vascular organ of lamina terminalis ;SuML, supramammillary nucleus, lateral part; SuMM, supramammillary nucleus, medial part;. **B**, Locations of brain nuclei receiving SFO^{CaMKII} neuronal projections (n=9 mice).

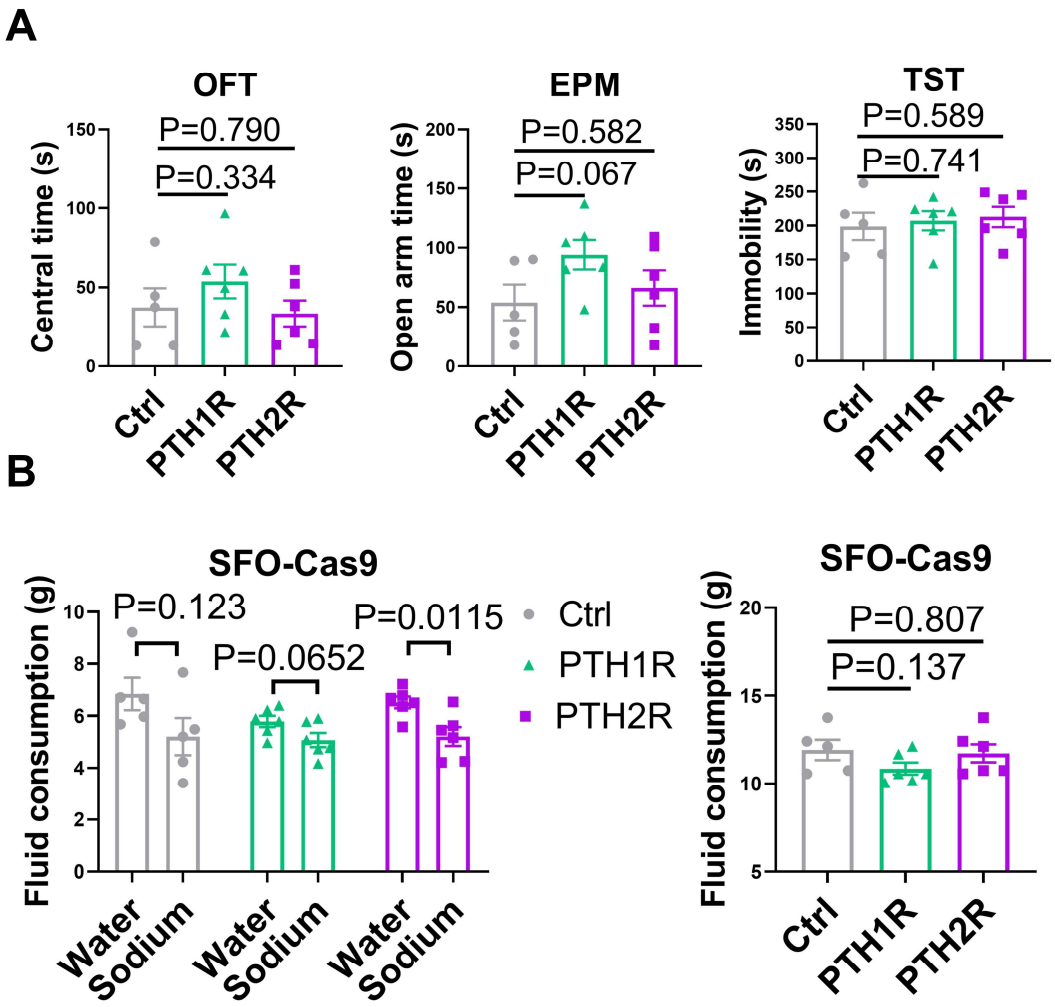

Supplementary figure 6. Behavioral and fluid-consumption tests of mice after knockdown of PTH1R/PTH2R expression in the SFO.

A, Behavioral tests in c57 mice after knockdown of PTH1R/PTH2R expression in the SFO. ***Left,*** time spent in the center during open field test. ***Middle***, open-arm time during elevated plus maze. ***Right***, immobility time during tail suspension test (n=5-6 mice for each chart). **B**. Fluid consumption (water or 0.3M NaCl) tests in c57 mice after knockdown of PTH1R/PTH2R expression in the SFO. ***Left,*** consumption of water and NaCl, ***right***, total fluid consumption (n=5-6 mice). P analyzed using paired two-tailed t-tests. All error bars and shaded areas show mean ± s.e.m.

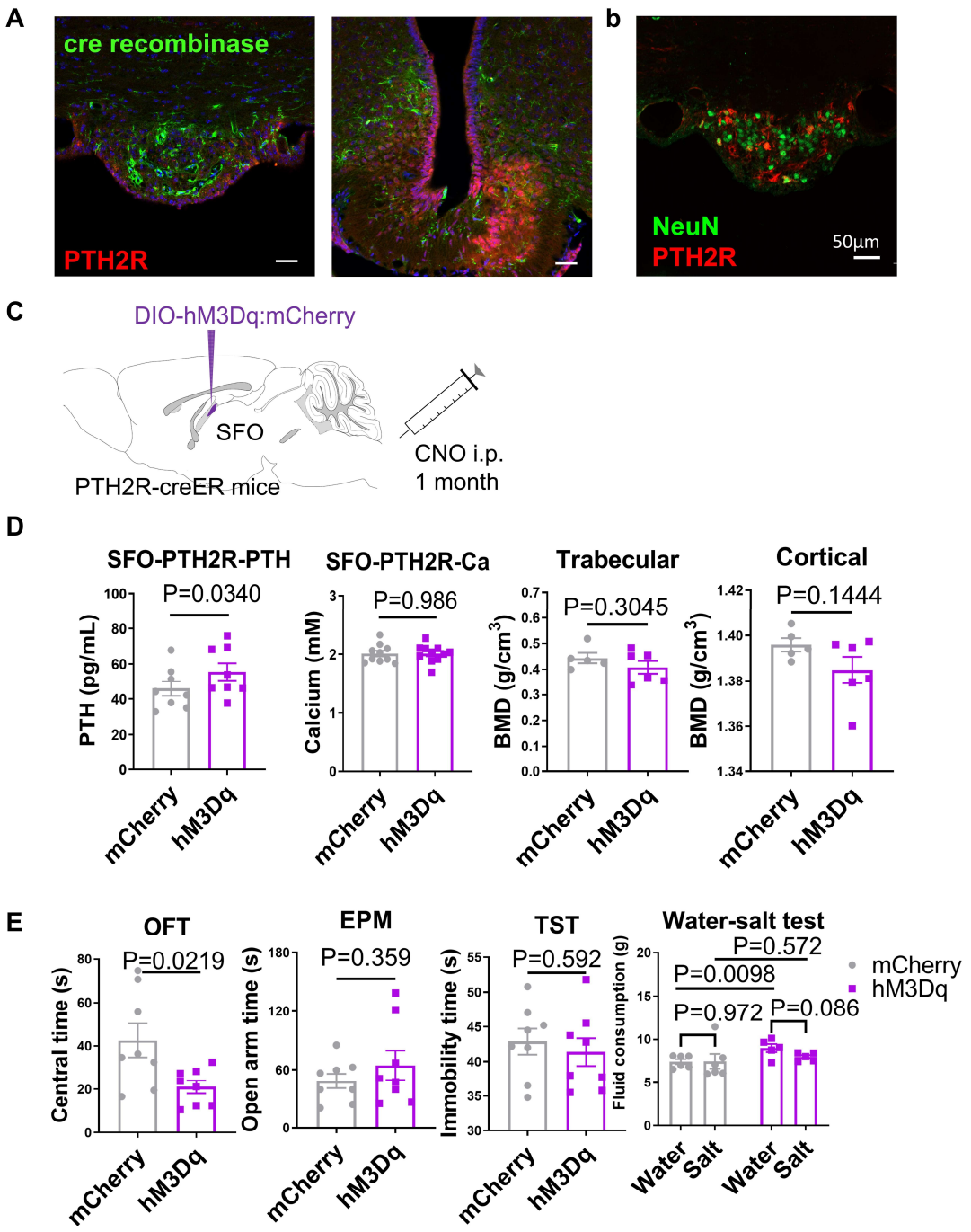

Supplementary figure 7. Chemogenetic stimulation of SFO^{PTH2R} neurons in PTH2R- CreERT2 mice.

A, Immunofluorescent staining against cre recombinase and PTH2R in SFO and median eminence (ME) of PTH2R-CreER^{T2} mice. Scale bar, 50 μm. **B**, PTH2R neurons labeled by injecting AAV-DIO-mCherry into the SFO of PTH2R-CreER^{T2} mice and colocalization with NeuN (green). Scale bar, 50 μm. (**C-E**) Chemogenetic activation of

PTH2R neurons in the SFO of PTH2R- CreER^{T2} mice (n=8 mice, scale bar, 50 μm). **C**, Injection of AAV-DIO-hM3Dq/mCherry into the SFO of PTH2R- CreER^{T2} mice followed with 1-month CNO *i.p.* administration. **D**, Serum PTH, total calcium level, tibia trabecular bone mineral density (BMD), and femur cortical BMD from MicroCT analysis. **E,** Behavioral tests after activation of SFO^{PTH2R} neurons. Time in center during open field test, open-arm time during elevated plus maze, immobility time during tail suspension test and fluid consumption quantity (water or 0.3M NaCl) were analyzed (n=8 mice). P analyzed using paired two-tailed t-test. All error bars and shaded areas show mean ± s.e.m.

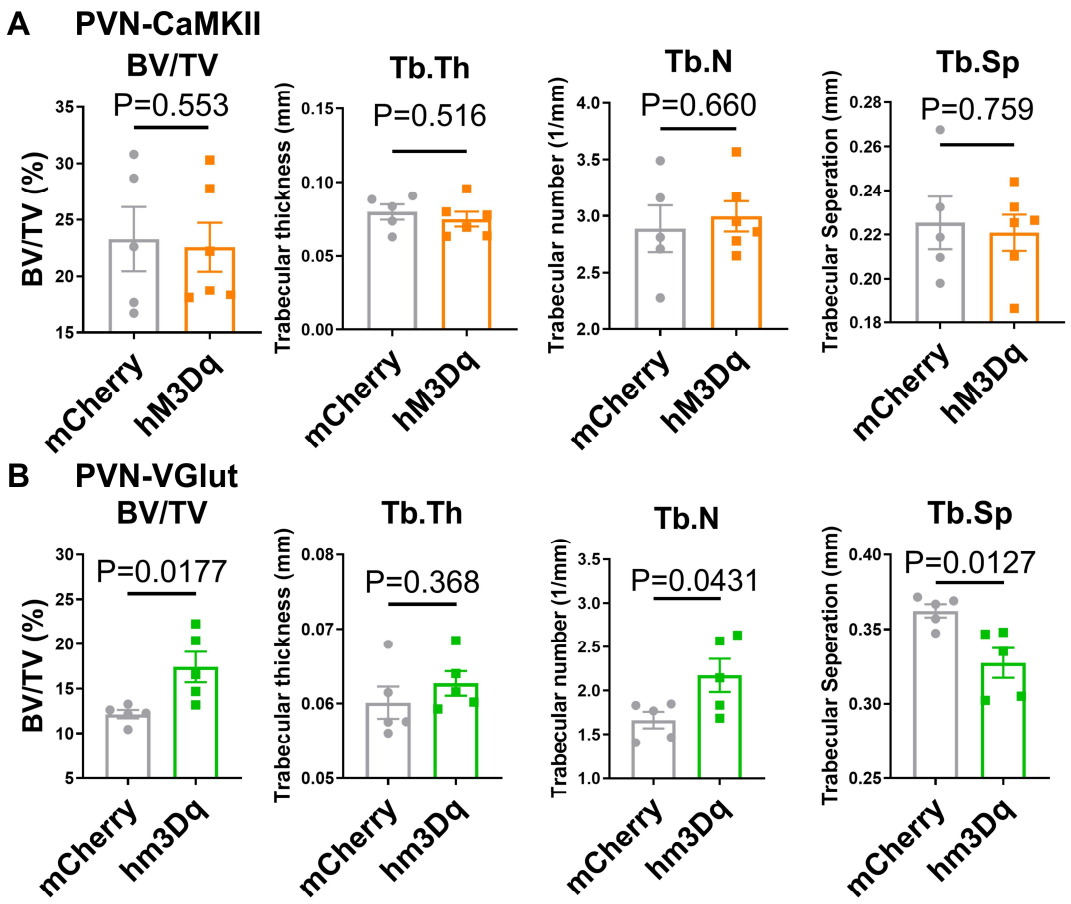

Supplementary figure 8. Bone analysis after chemogenetic stimulation of PVN neurons.

A, The tibia trabecular percent bone volume (BV/TV), trabecular thickness (Tb.Th), trabecular numbers (Tb.N), trabecular separation (Tb.Sp) assessed by MicroCT analysis after chemogenetic stimulation of PVN^{CaMKII} neurons for 1 month in C57 mice (n=5-6 mice). **B,** Tibia trabecular BV/TV, Tb.Th, Tb.N and Tb.Sp assessed by MicroCT analysis after chemogenetic stimulation of PVN^{VGlut} neurons in VGlut2-cre mice (n=5 mice). P analyzed using paired two-tailed t-test. All error bars and shaded areas show mean ± s.e.m.

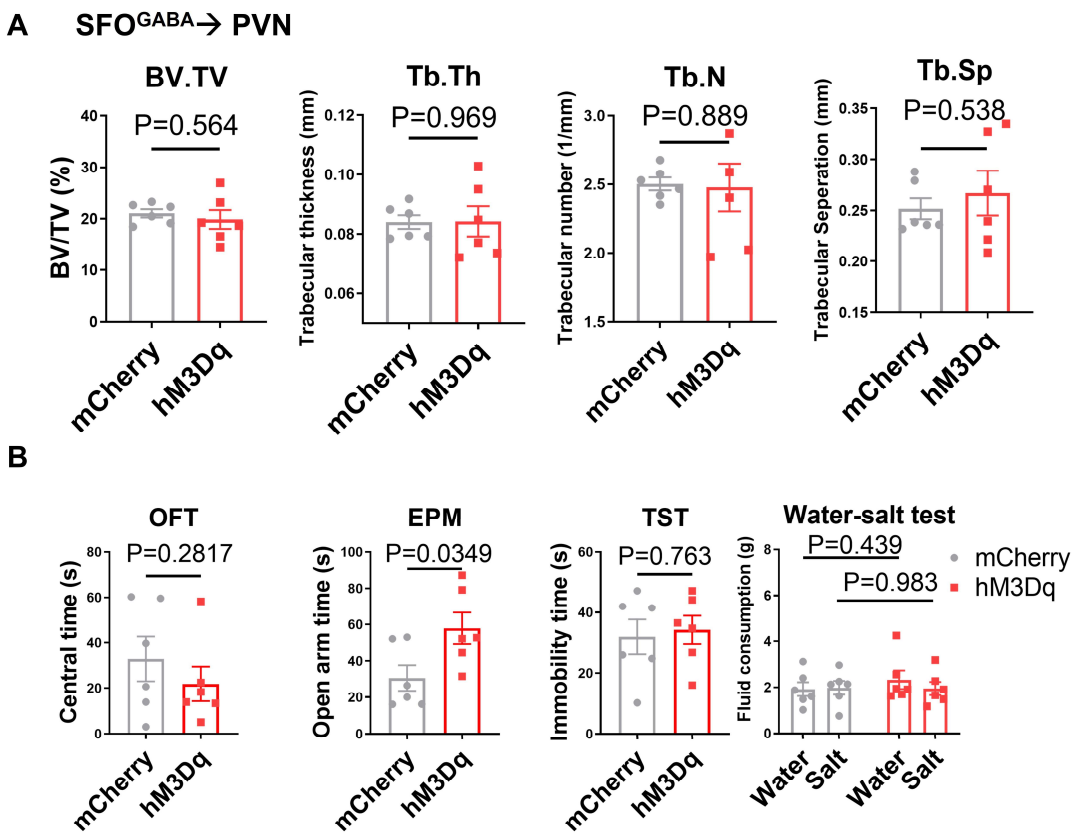

Supplementary figure 9. Bone analysis and behavioral tests following stimulation of the SFO^{GAD}→PVN neural circuit

A, Tibia trabecular percent bone volume (BV/TV), trabecular thickness (Tb.Th), trabecular numbers (Tb.N), trabecular separation (Tb.Sp) assessed by MicroCT analysis after chemogenetic stimulation of SFO^{GAD}→PVN for 1 month in C57 mice (n=6 mice). **B**, Behavioral tests after activation of the SFO^{GAD}→PVN neural circuit. Time in center during an open field test, open-arm time during the elevated plus maze test, immobility time during tail suspension test, and fluid consumption (water or 0.3 M NaCl) were compared amongst groups (n=6 mice/group). P analyzed using paired two-tailed t-test. All error bars and shaded areas show mean ± s.e.m.

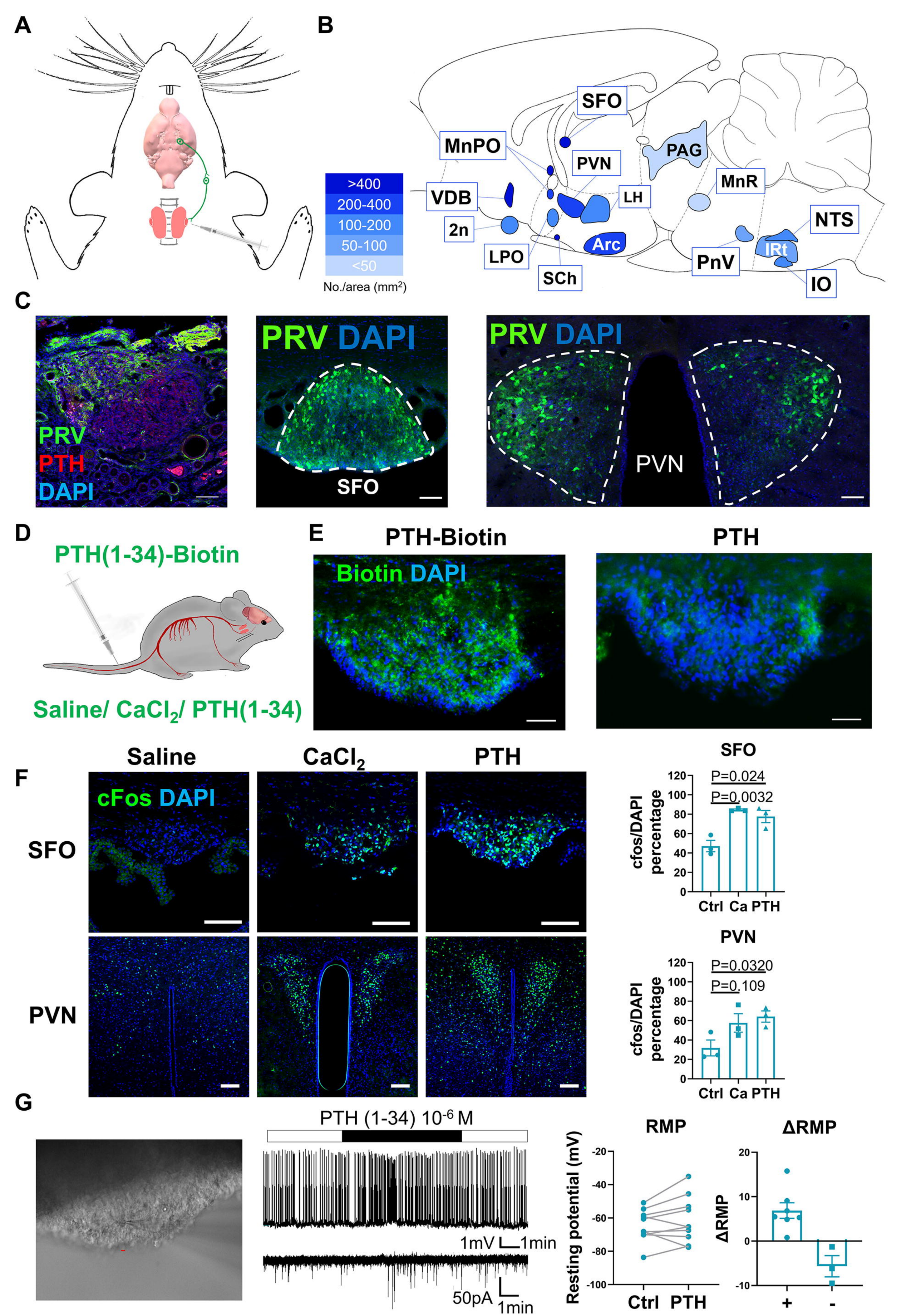
A
B
>400
200-400
100-200
50-100
<50
No./area (mm²)
SFO
MnPO
PVN
PAG
VDB
LH
MnR
2n
NTS
Arc
LPO
IRt
PnV
SCh
IO
C
PRV
PTH
DAPI
PRV DAPI
SFO
PRV DAPI
PVN
D
PTH(1-34)-Biotin
Saline/ CaCl2/ PTH(1-34)
E
PTH-Biotin
Biotin DAPI
PTH
F
Saline
CaCl2
PTH
cFos DAPI
SFO
PVN
SFO
P=0.024
P=0.0032
cfos/DAPI percentage
Ctrl Ca PTH
PVN
P=0.0320
P=0.109
cfos/DAPI percentage
Ctrl Ca PTH
G
PTH (1-34) 10-6 M
1mV
1min
50pA
1min
RMP
Resting potential (mV)
Ctrl PTH
ΔRMP
ΔRMP
+
-

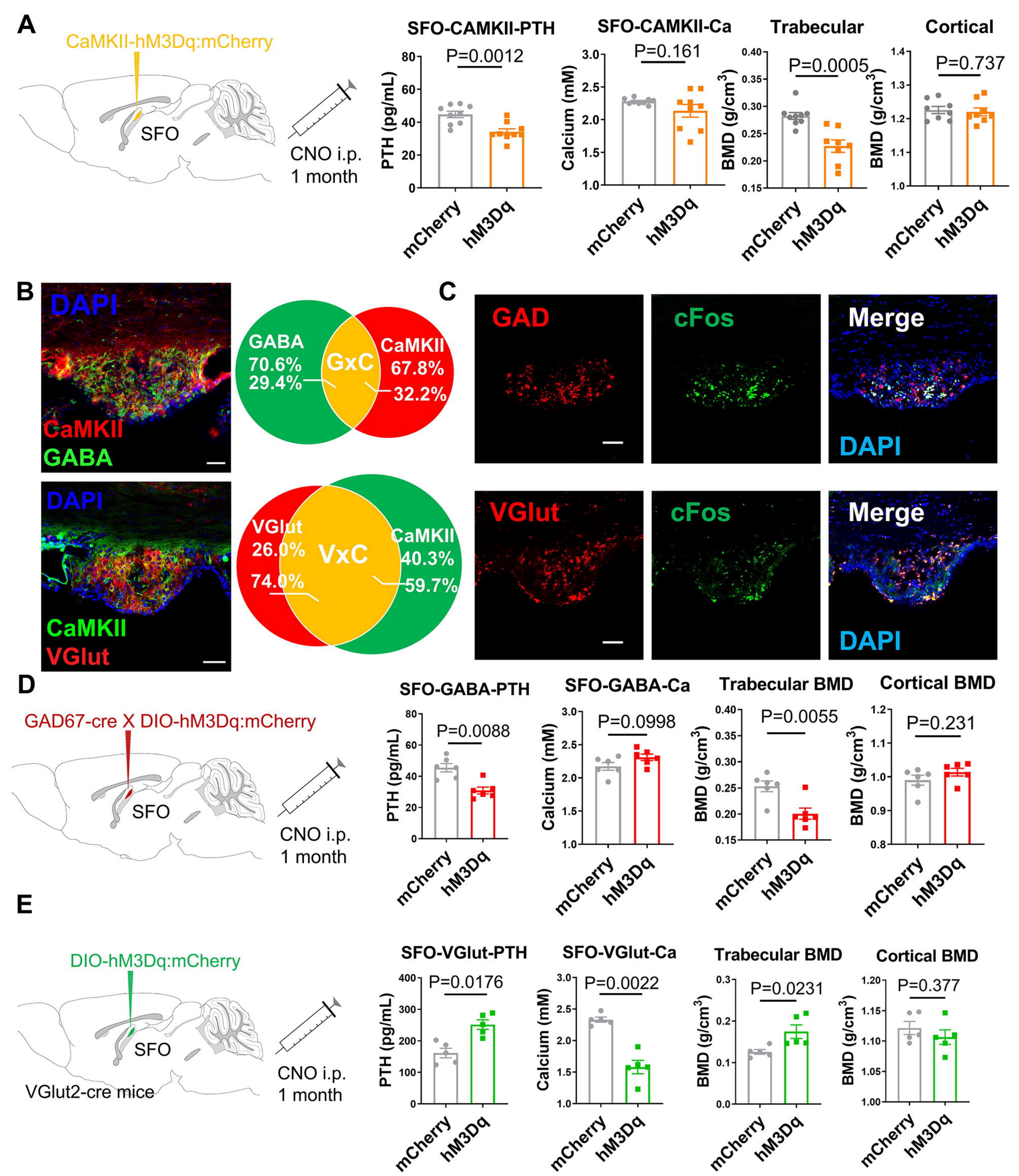
A
CaMKII-hM3Dq:mCherry
SFO
CNO i.p.
1 month
SFO-CAMKII-PTH
P=0.0012
PTH (pg/mL)
SFO-CAMKII-Ca
P=0.161
Calcium (mM)
Trabecular
P=0.0005
BMD (g/cm3)
Cortical
P=0.737
BMD (g/cm3)
mCherry
hM3Dq
B
DAPI
CaMKII
GABA
GABA
70.6%
29.4%
GxC
CaMKII
67.8%
32.2%
DAPI
CaMKII
VGlut
VGlut
26.0%
74.0%
VxC
CaMKII
40.3%
59.7%
C
GAD
cFos
Merge
DAPI
VGlut
cFos
Merge
DAPI
D
GAD67-cre X DIO-hM3Dq:mCherry
SFO
CNO i.p.
1 month
SFO-GABA-PTH
P=0.0088
PTH (pg/mL)
SFO-GABA-Ca
P=0.0998
Calcium (mM)
Trabecular BMD
P=0.0055
BMD (g/cm3)
Cortical BMD
P=0.231
BMD (g/cm3)
mCherry
hM3Dq
E
DIO-hM3Dq:mCherry
SFO
VGlut2-cre mice
CNO i.p.
1 month
SFO-VGlut-PTH
P=0.0176
PTH (pg/mL)
SFO-VGlut-Ca
P=0.0022
Calcium (mM)
Trabecular BMD
P=0.0231
BMD (g/cm3)
Cortical BMD
P=0.377
BMD (g/cm3)
mCherry
hM3Dq

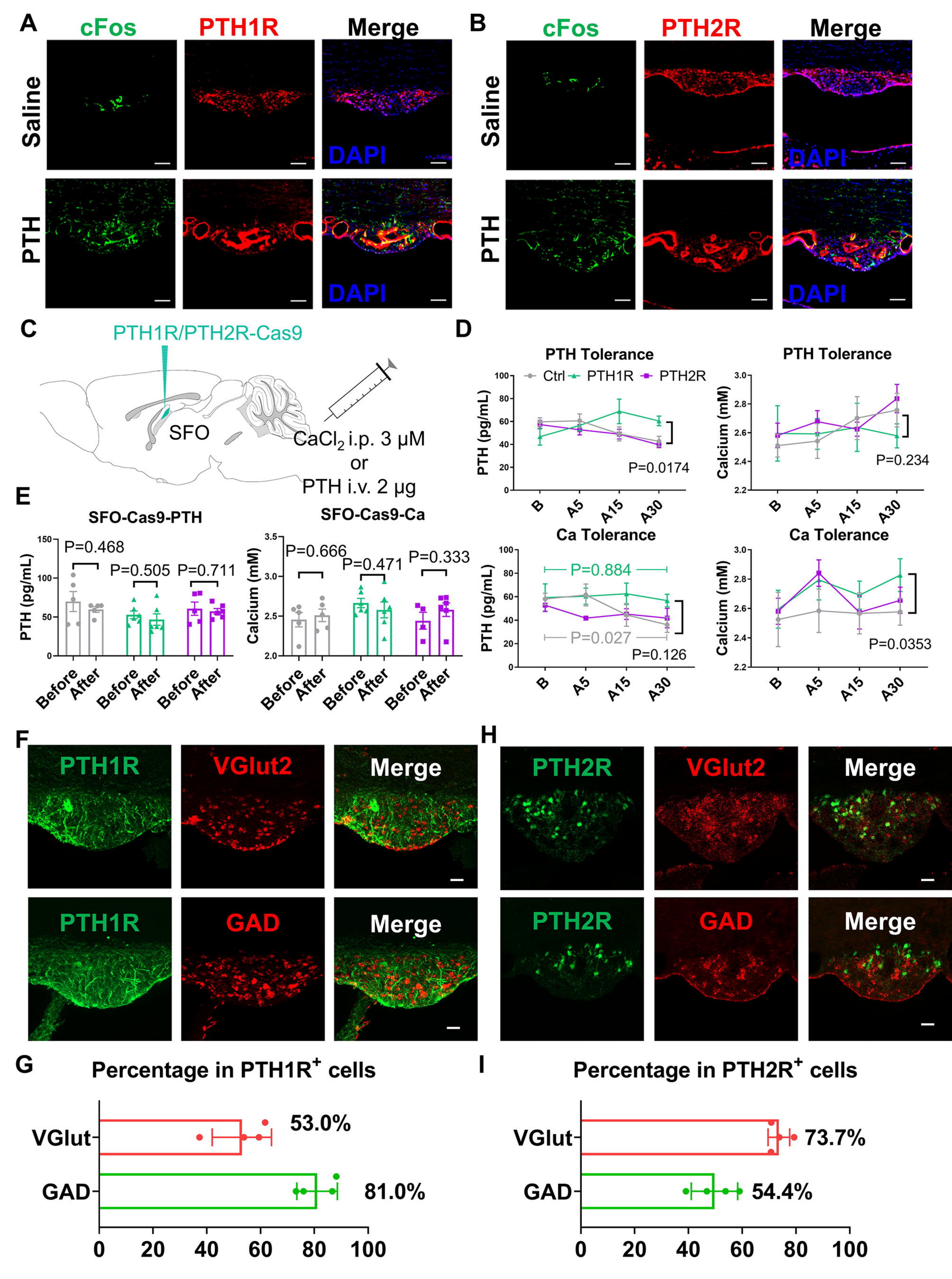
A
cFos
PTH1R
Merge
Saline
PTH
DAPI
B
cFos
PTH2R
Merge
Saline
PTH
DAPI
C
PTH1R/PTH2R-Cas9
SFO
CaCl2 i.p. 3 μM
or
PTH i.v. 2 μg
D
PTH Tolerance
Ctrl
PTH1R
PTH2R
PTH (pg/mL)
P=0.0174
B
A5
A15
A30
PTH Tolerance
Calcium (mM)
P=0.234
Ca Tolerance
PTH (pg/mL)
P=0.884
P=0.027
P=0.126
Ca Tolerance
Calcium (mM)
P=0.0353
E
SFO-Cas9-PTH
PTH (pg/mL)
P=0.468
P=0.505
P=0.711
Before
After
SFO-Cas9-Ca
Calcium (mM)
P=0.666
P=0.471
P=0.333
F
PTH1R
VGlut2
Merge
PTH1R
GAD
Merge
H
PTH2R
VGlut2
Merge
PTH2R
GAD
Merge
G
Percentage in PTH1R+ cells
VGlut
53.0%
GAD
81.0%
I
Percentage in PTH2R+ cells
VGlut
73.7%
GAD
54.4%

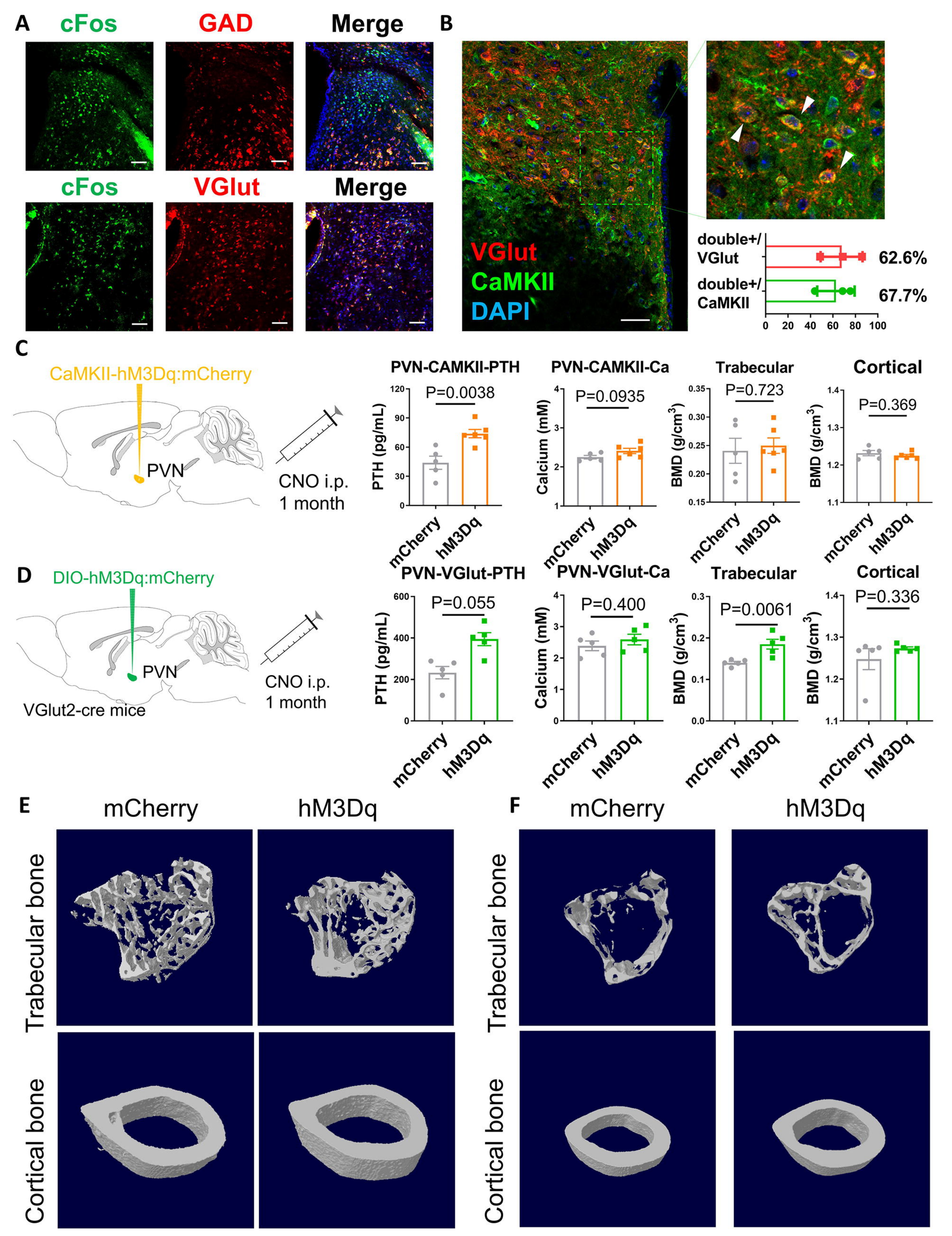
A
cFos
GAD
Merge
cFos
VGlut
Merge
B
VGlut
CaMKII
DAPI
double+/ VGlut
62.6%
double+/ CaMKII
67.7%
0 20 40 60 80 100
C
CaMKII-hM3Dq:mCherry
PVN
CNO i.p.
1 month
PVN-CAMKII-PTH
PVN-CAMKII-Ca
Trabecular
Cortical
P=0.0038
P=0.0935
P=0.723
P=0.369
PTH (pg/mL)
Calcium (mM)
BMD (g/cm3)
mCherry
hM3Dq
D
DIO-hM3Dq:mCherry
PVN
VGlut2-cre mice
CNO i.p.
1 month
PVN-VGlut-PTH
PVN-VGlut-Ca
Trabecular
Cortical
P=0.055
P=0.400
P=0.0061
P=0.336
PTH (pg/mL)
Calcium (mM)
BMD (g/cm3)
mCherry
hM3Dq
E
mCherry
hM3Dq
Trabecular bone
Cortical bone
F
mCherry
hM3Dq
Trabecular bone
Cortical bone

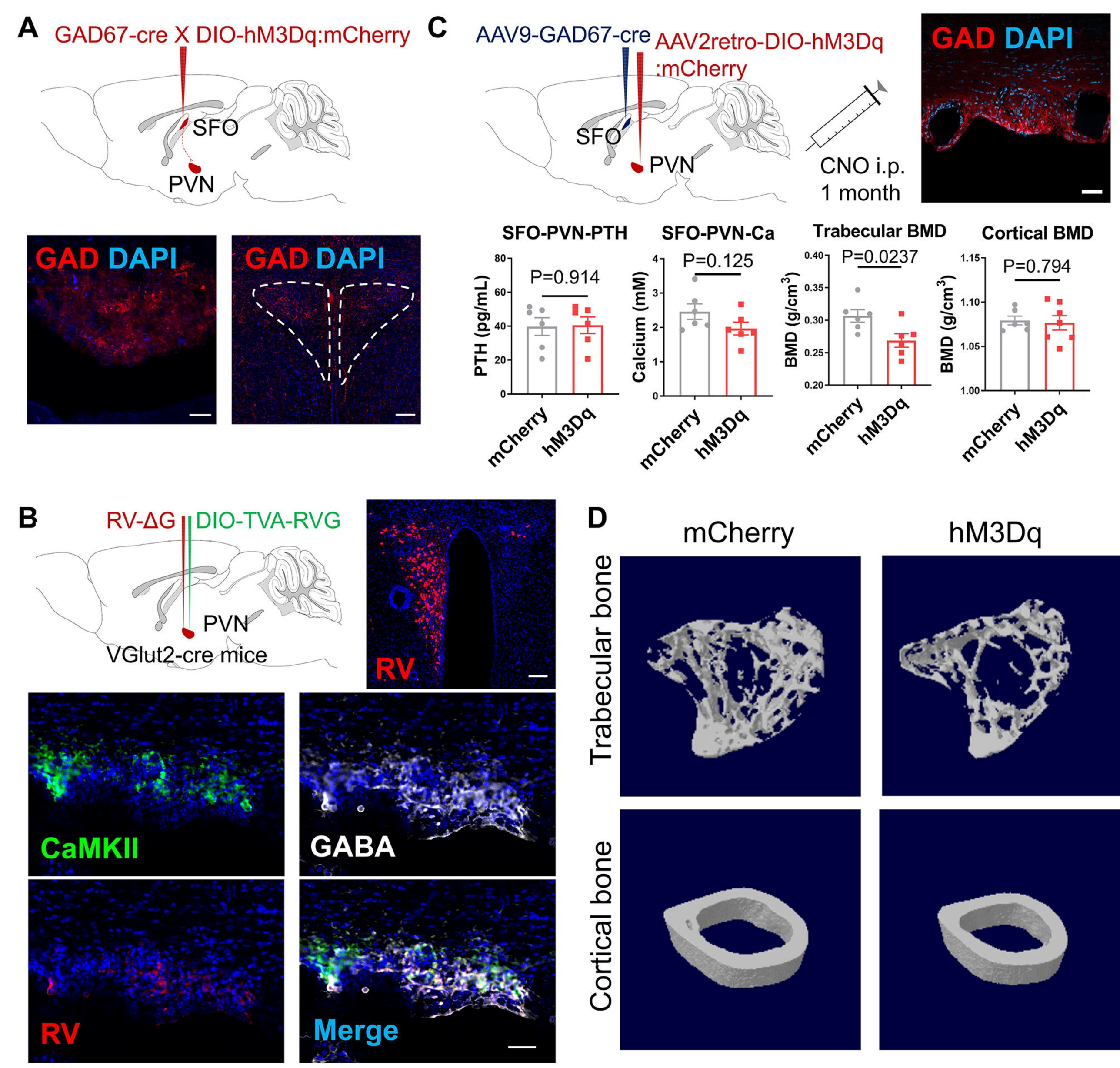
A
GAD67-cre X DIO-hM3Dq:mCherry
SFO
PVN
GAD DAPI
GAD DAPI
B
RV-ΔG
DIO-TVA-RVG
PVN
VGlut2-cre mice
RV
CaMKII
GABA
RV
Merge
C
AAV9-GAD67-cre
AAV2retro-DIO-hM3Dq
:mCherry
SFO
PVN
CNO i.p.
1 month
GAD DAPI
SFO-PVN-PTH
PTH (pg/mL)
P=0.914
mCherry
hM3Dq
SFO-PVN-Ca
Calcium (mM)
P=0.125
mCherry
hM3Dq
Trabecular BMD
BMD (g/cm3)
P=0.0237
mCherry
hM3Dq
Cortical BMD
BMD (g/cm3)
P=0.794
mCherry
hM3Dq
D
mCherry
hM3Dq
Trabecular bone
Cortical bone

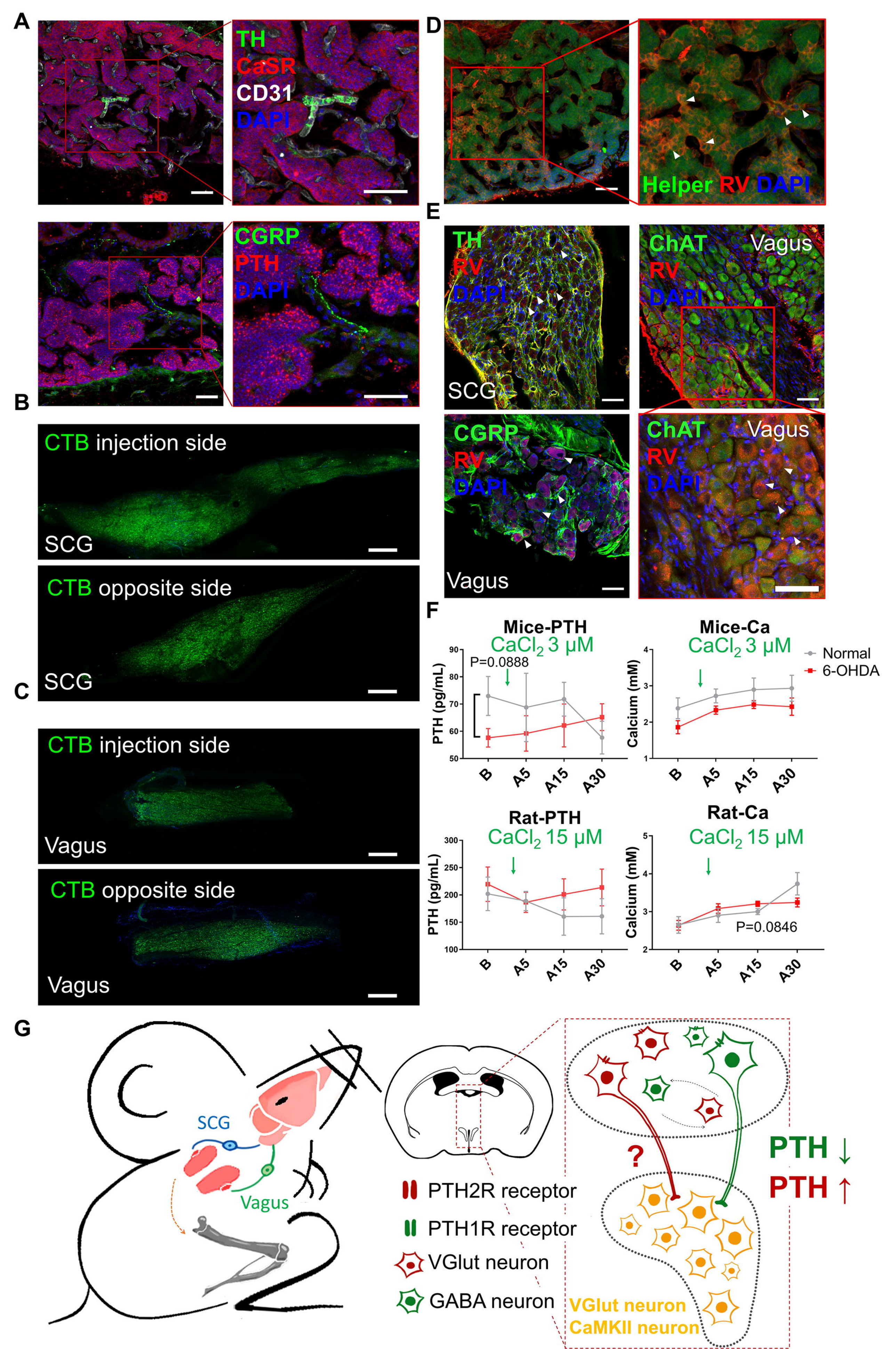
A
TH
CaSR
CD31
DAPI
B
CGRP
PTH
DAPI
C
CTB injection side
SCG
CTB opposite side
SCG
CTB injection side
Vagus
CTB opposite side
Vagus
D
Helper RV DAPI
E
TH
RV
DAPI
SCG
ChAT
Vagus
RV
DAPI
CGRP
RV
DAPI
Vagus
ChAT
Vagus
RV
DAPI
F
Mice-PTH
CaCl2 3 μM
P=0.0888
PTH (pg/mL)
Mice-Ca
CaCl2 3 μM
Calcium (mM)
Normal
6-OHDA
B
A5
A15
A30
Rat-PTH
CaCl2 15 μM
PTH (pg/mL)
Rat-Ca
CaCl2 15 μM
Calcium (mM)
P=0.0846
G
SCG
Vagus
PTH2R receptor
PTH1R receptor
VGlut neuron
GABA neuron
?
PTH ↓
PTH ↑
VGlut neuron
CaMKII neuron